

The Standardizability of Type Ia Supernovae in the Near-Infrared: Evidence for a Peak Luminosity Versus Decline-Rate Relation in the Near-Infrared

ShiAnne Kattner

Department of Astronomy, San Diego State University, San Diego, CA 92182-1221, U.S.A.

skattner@sciences.sdsu.edu

Douglas C. Leonard

Department of Astronomy, San Diego State University, San Diego, CA 92182-1221, U.S.A.

leonard@sciences.sdsu.edu

Christopher R. Burns

Observatories of the Carnegie Institution for Science, 813 Santa Barbara St., Pasadena, CA 91101, U.S.A.

crburns@me.com

M. M. Phillips

Carnegie Observatories, Las Campanas Observatory, Colina El Pino, Casilla 601, La Serena, Chile

mmp@lco.cl

Gastón Folatelli

Institute for the Physics and Mathematics of the Universe (IPMU), University of Tokyo, 5-1-5 Kashiwanoha, Kashiwa, Chiba 277-8583, Japan

gaston.folatelli@ipmu.jp

Nidia Morrell

Carnegie Observatories, Las Campanas Observatory, Colina El Pino, Casilla 601, La Serena, Chile

nmorrell@lco.cl

Maximilian D. Stritzinger

*The Oskar Klein Centre, Department of Astronomy, Stockholm University, AlbaNova,
10691 Stockholm, Sweden*

`max.stritzinger@astro.su.se`

*Dark Cosmology Centre, Niels Bohr Institute, University of Copenhagen, Juliane Maries
Vej 30, 2100 Copenhagen Ø*

`max@dark-cosmology.dk`

*Carnegie Observatories, Las Campanas Observatory, Colina El Pino, Casilla 601, La
Serena, Chile*

`mstritzinger@lco.cl`

Mario Hamuy

Departamento de Astronomía, Universidad de Chile, Casilla 36-D, Santiago, Chile

`mhamuy@das.uchile.cl`

Wendy L. Freedman

*Observatories of the Carnegie Institution for Science, 813 Santa Barbara St., Pasadena,
CA 91101, U.S.A.*

`wendy@obs.carnegiescience.edu`

Sven E. Persson

*Observatories of the Carnegie Institution for Science, 813 Santa Barbara St., Pasadena,
CA 91101, U.S.A.*

`persson@obs.carnegiescience.edu`

Miguel Roth

*Carnegie Observatories, Las Campanas Observatory, Colina El Pino, Casilla 601, La
Serena, Chile*

`miguel@lco.cl`

Nicholas B. Suntzeff

*George P. and Cynthia Woods Mitchell Institute for Fundamental Physics and Astronomy,
Department of Physics and Astronomy, Texas A&M University, College Station, TX
77843, USA*

nsuntzeff@tamu.edu

ABSTRACT

We analyze the standardizability of Type Ia supernovae (SNe Ia) in the near-infrared (NIR) by investigating the correlation between observed peak NIR (YJH) absolute magnitude and post-maximum B -band decline-rate $[\Delta m_{15}(B)]$. A sample of 27 low-redshift SNe Ia with well-observed NIR light-curves observed by the *Carnegie Supernova Project* (CSP) between 2004 and 2007 is used. All 27 objects have pre-maximum coverage in optical bands, with a subset of 13 having pre-maximum NIR observations as well; coverage of the other 14 begins shortly after NIR maximum brightness. We describe the methods used to derive light-curve parameters (absolute peak magnitudes and decline-rates) from both spline and template fitting procedures, and confirm prior findings that fitting templates to SNe Ia light-curves in the NIR is problematic due to the diversity of post-maximum behavior of objects that are characterized by similar $\Delta m_{15}(B)$ values, especially at high decline-rates. Nevertheless, we show that NIR light-curves can be reasonably fit with a template, especially if the observations begin within 5 days after NIR maximum. SNe Ia appear to be better “standardizable candles” in the NIR bands than in the optical bands. For the subset of 13 objects in our data set that excludes the highly reddened and fast-declining SNe Ia, and includes only those objects for which NIR observations began prior to 5 days after maximum light, we find modest (1.7σ) evidence for a peak luminosity vs. decline-rate relation in Y , and stronger evidence (2.8σ) in J and H . Using R_V values differing from the canonical value ($R_V = 3.1$) is shown to have little effect on the results. A Hubble diagram is presented for the NIR bands and the B -band. The resulting scatter for the combined NIR bands is 0.13 mag, while the B -band produces a scatter of 0.22 mag. Finally, we find evidence for a bimodal distribution in the NIR absolute magnitudes of fast-declining SNe Ia $[\Delta m_{15}(B) > 1.7]$. These data suggest that applying a correction to SNe Ia peak luminosities for decline-rate is likely to be beneficial in the J - and H -bands to make SNe Ia more precise distance indicators, but of only marginal importance in the Y -band.

Subject headings: Supernovae

1. Introduction

It is widely accepted that SNe Ia are excellent *standardizable candles* at optical wavelengths. After applying an empirical correction established between light-curve shape and peak magnitude, SNe Ia become one of the most precise extragalactic distance indicators known. Phillips (1993) was the first to discover a tight correlation (hereafter the “Phillips method”) between optical absolute magnitudes at maximum light and the decline-rate parameter $\Delta m_{15}(B)$, defined as the drop in B -band brightness from peak to 15 days later. Slow-declining SNe Ia [i.e., lower $\Delta m_{15}(B)$] are intrinsically brighter than their fast-declining counterparts. Since Phillips’ initial work, the Phillips method has continued to be utilized (Hamuy et al. 1996; Phillips et al. 1999; Prieto et al. 2006; Burns et al. 2011), along with other similar calibration methods, such as the “stretch” method (Perlmutter et al. 1997; Goldhaber et al. 2001), the multicolor light-curve shape method (MLCS/MLCS2k2; Riess et al. 1996, 1998; Jha et al. 2007), the color-magnitude intercept calibration method (CMAGIC; Wang et al. 2003), the spectral adaptive light-curve template method (SALT/SALT2; Guy et al. 2005, 2007), and SiFTO (Conley et al. 2008). Applying such corrections decreases the dispersion in measured distance estimates to the 0.20 mag level or less (Hamuy et al. 1996; Prieto et al. 2006; Wood-Vasey et al. 2008; Folatelli et al. 2010), which significantly improves the accuracy of SNe Ia as standardizable candles at optical wavelengths.

SNe Ia have played a critical role in cosmological studies over the past two decades. While the majority of SNe Ia studies have been performed using optical bands, there has long been the hope that they might actually have greater accuracy in NIR bands, due to the reduced effects of dust extinction, which is one of the main sources of error in distance determinations (Freedman et al. 2009). This has motivated recent work on establishing the standardizability of SNe Ia in the NIR, which has been shown to be advantageous for several reasons. Extinction corrections are smaller, on the order of a magnitude less, in NIR than in optical bands (Cardelli et al. 1989), and there appears to be a shallower dependence of absolute NIR magnitude on decline-rate compared with optical bands (Krisciunas et al. 2004a,c; Wood-Vasey et al. 2008; Mandel et al. 2010; Folatelli et al. 2010). Recently, Gallagher et al. (2008), Sullivan et al. (2010), and Kelly et al. (2010) have found that the absolute magnitudes of SNe Ia depend on host-galaxy properties (i.e., star formation rate, host-galaxy mass, host-galaxy metallicity), making the correction factors evolve with redshift. Therefore, minimizing these correction factors by observing in the NIR is important, not only to decrease the random errors incurred for each SN Ia’s correction, but also to reduce our sensitivity to any systematic evolution of the correction factors with redshift.

The first NIR observation of a SN Ia was reported by Kirshner et al. (1973), and the first extensive NIR data set was obtained by Elias et al. (1981, 1985). Since that time, there

has been a large increase in the number of SNe Ia light-curves observed at NIR wavelengths, especially within the last decade (e.g., Frogel et al. 1987; Jha et al. 1999; Phillips et al. 2003; Krisciunas et al. 2004a,b,c, 2006; Stritzinger & Sollerman 2007; Wood-Vasey et al. 2008; Contreras et al. 2010; Stritzinger et al. 2011 and references therein). Two groups, in particular, have been working to obtain homogenous optical and NIR data sets of SNe of all types in multiple filters: the CfA Supernova Group (Wood-Vasey et al. 2008) and the *Carnegie Supernova Project* (CSP; Hamuy et al. 2006).

Initial studies suggested that SNe Ia may present a weaker peak luminosity vs. decline-rate dependence in the NIR compared with the optical, which display slopes of 0.63, 0.61, 0.57, and 0.52 mag unit⁻¹ decline-rate [as measured by $\Delta m_{15}(B)$] in *BVRI*, respectively (Prieto et al. 2006). This led some early investigators (e.g., Elias et al. 1985; Phillips 1993; Meikle 2000) to suggest that these objects may be nearly perfect standard candles in the NIR. Krisciunas et al. (2004a,c) confirmed these suggestions, finding no obvious decline-rate relations in the *JHK_s* bands, concluding that SNe Ia might well be nearly perfect standard candles in the NIR at the ± 0.20 mag level or better. A study by Wood-Vasey et al. (2008), which did not correct for optical light-curve shape, found SNe Ia to be excellent standard candles in the NIR, deriving an intrinsic dispersion in absolute magnitude of only 0.28 mag in the *J*-band and 0.15 mag in the *H*-band. Folatelli et al. (2010) found a marginal dependence of absolute NIR magnitudes on decline-rate using CSP SNe Ia (0.44 ± 0.14 , 0.58 ± 0.09 , 0.33 ± 0.18 mag unit⁻¹ decline-rate in *YJH*, respectively). Some of these earlier studies, however, employ inhomogeneous samples of SNe Ia (e.g., different telescopes, different reduction procedures), so subtle systematics may complicate interpretation of the results.

In this article we re-examine the standardizability of SNe Ia in the NIR bands using a homogeneously obtained sample of 27 low-redshift objects observed by the CSP between 2004 and 2007. We use these data to quantitatively examine whether a decline-rate dependence correction is needed in the NIR or whether SNe Ia are indeed perfect standard candles at these wavelengths. A detailed description of the CSP observations, data reduction, and photometry processes can be found in Hamuy et al. (2006) and Contreras et al. (2010). All of the photometric data are on the Swope+CSP natural photometric system, with the final SN photometry published by Contreras et al. (2010), with the exception of three SNe Ia (SNe 2006et, 2007af, and 2007on) whose photometry are presented in the second CSP data release article (Stritzinger et al. 2011).

This article is organized as follows. In §2 we briefly discuss light-curve template-fitting using SNooPy (SuperNova in Object-Oriented Python; Burns et al. 2011), and we point out difficulties with the template-fitting approach. In §3 we examine the standardizability of

SNe Ia in NIR bands by examining the efficacy of the Phillips method to fit the relationship between absolute peak Y , J , and H magnitudes and decline-rates. In §4 we investigate the bimodal distribution of the fast-declining, low-luminosity SNe at these wavelengths. We summarize our conclusions in §5.

2. NIR Light-Curve Fitting and Morphology

2.1. Light-Curve Fitting Using SNooPy

From 2004–2007, the CSP obtained ~ 100 SN Ia light-curves in both optical and NIR bands. Here, we choose 27 of the best-observed objects discovered during the first three campaigns, all of which have optical observations that start before maximum light and continue for at least 30 days post-maximum. Thirteen of the SNe Ia have NIR observations that begin before maximum brightness as well, while the others begin shortly after maximum brightness. We denote a best-fit (BF) subsample as those 13 objects with observed maxima in both optical and NIR bands. This BF subsample is used to create a “training set” for the template light-curves following the process described here.

SN Ia light-curve parameters are typically measured with respect to the peak of the light-curve. We prefer to directly measure the K -corrected, de-reddened time of maximum (t_X^{max}), peak magnitude (m_X^{max}), and decline-rate [$\Delta m_{15}(B)$] based on a cubic-spline interpolation of the data points themselves (see the discussion in Burns et al. 2011). However, in $YJHK_s$, SNe Ia typically achieve peak brightness 3–4 days prior to B -band maximum, which often results in having objects with well-observed optical peaks but NIR observations that begin post-peak. Although not optimal, peak values (i.e., t_X^{max} and m_X^{max}) can be estimated for such objects by fitting their post-peak data with a template light-curve based on observations of SNe Ia with well-observed optical and NIR peaks.

To generate and fit our templates, we employ the SNooPy package (Burns et al. 2011). To create the training set using the best-observed objects, SNooPy examines the B -band light-curves and computes where the derivative is zero on the cubic-spline fit. This point is used to estimate t_X^{max} and m_X^{max} (and their uncertainties). Once t_B^{max} is found, SNooPy measures $\Delta m_{15}(B)$ and then m^{max} in all of the other filters. This training set of SNe Ia is then used to create the template $ugriBVYJH$ light-curves through the procedure detailed by Burns et al. (2011). Briefly, t^{max} , m^{max} , and $\Delta m_{15}(B)$ of the training set are placed on a three-dimensional surface for each band. SNooPy interpolates across the surface along a constant $\Delta m_{15}(B)$ line using a 2D variation of the Gloess algorithm (Persson et al. 2004). From the template light-curves, SNooPy then measures the best-fit values of t^{max} , m^{max} , and

Δm_{15} , which is the template-derived value of the decline-rate derived from a combination of all filters, via χ^2 minimization. For consistency, we use $\Delta m_{15}(B)$, which is the decline-rate directly measured from the B -band, as the decline-rate parameter for all of our objects in all filters, including those objects that were template fit. The measured $\Delta m_{15}(B)$ parameters for all SNe are listed in Table 1.

2.2. Light-Curve Morphology and the Second Maximum in the NIR

Unlike optical light-curves, which are quite homogeneous for a fixed $\Delta m_{15}(B)$, light-curves at longer wavelengths display a more diverse morphology, particularly due to the existence of a rise to a “second maximum” following the initial peak. Investigation in the i -band has shown that this second peak can exhibit a strength and morphology that varies significantly from SN Ia to SN Ia with identical $\Delta m_{15}(B)$ values (e.g., Freedman et al. 2009; Folatelli et al. 2010; Burns et al. 2011). We confirm this with our sample in YJH (see Figs. 1 and 2). Note the similarity in the B and V light-curves in Figures 1 and 2 and the difference in the YJH light-curves, especially around the second maximum. This creates a problem for template fitting NIR light-curves using a one-parameter descriptor of light-curve shape, especially for fast-declining SNe Ia [i.e., $\Delta m_{15}(B) > 1.7$].

To test the accuracy of light-curve parameters derived from template fits, we compare the peak YJH magnitudes obtained from template fits with those obtained directly from spline fits for the BF group [excluding SNe with $\Delta m_{15}(B) > 1.7$] in Figure 3. The weighted averages of the difference in peak magnitude for YJH are 0.02 mag, 0.02 mag, and 0.05 mag, respectively, for objects with $\Delta m_{15}(B) < 1.7$. Figure 3 shows evidence of systematic differences, particularly in H , but the systematic errors are not large compared with the uncertainties in the final absolute magnitudes due to the errors in the host color excess and the derived distances.

Folatelli et al. (2010) also found evidence of systematic differences in peak magnitudes derived from template vs. spline fits for the NIR filters, as shown in their Figure 5, stating that the poor precision of the template fit in $iYJH$ is partly due to the small sample used to derive the templates and also due to the variation in morphology surrounding the second maximum. Burns et al. (2011) used a bootstrap technique to incorporate the extra dispersion found in the template fits caused by NIR light-curve variations. We have attempted to account for this extra dispersion by adding the extrapolation errors derived by Burns et al. (2011) in quadrature with the uncertainties in the apparent magnitude obtained from the SNooPy fits.

Because the variations in the strength of the secondary maximum affect the accuracy of light-curve template fitting in the $iYJH$ bands, we might expect the uncertainties in the peak NIR magnitudes to be a function of how many days past maximum the observations begin. Folatelli et al. (2010) found that if a SNe Ia has observations that begin within ~ 1 week after the time of maximum, the random uncertainty in peak magnitude is ~ 0.1 mag and the systematic uncertainty is only ~ 0.03 mag; a template fit for a SNe Ia with photometry that starts later than this will be unreliable. Two thirds of the events in our sample with $\Delta m_{15}(B) < 1.7$ have photometry that starts within 5 days of the NIR maximum, and so it is interesting to see if the template fitting procedure gives reasonable estimates of the peak magnitude for these SNe Ia. To test this, we create a plot similar to that of Figure 3. For this test, we re-derive the template fit peak NIR apparent magnitudes by removing all of the data prior to 5 days after NIR maximum for each SN Ia and running the data through SNooPy again. Figure 4 shows the resulting plots in YJH . There appear to be some systematic differences, but, again, they are not large when compared with the uncertainties in the final absolute magnitudes. The weighted averages of the differences are 0.03 mag in Y , 0.01 mag in J , and 0.04 mag in H , which is about the same for the weighted averages found in Figure 3, suggesting that when the observations begin within 5 days of NIR maximum, SNooPy does an adequate job of deriving peak light-curve parameters from template fits.

It is unclear at this point how to best handle the diversity of light-curve morphologies in the NIR when applying templates to SNe Ia whose NIR observations start more than 5 days after NIR maxima. Introducing a second parameter, such as another peak magnitude, decline-rate relation (such as a Δm_{15} -like parameter defined for the YJH bandpasses), host-galaxy property, or spectral feature, might help (e.g., Kasen 2006; Wang et al. 2009; Foley & Kasen 2011; Sullivan et al. 2010; Blondin et al. 2011), but identifying this second parameter is difficult with the limited number of well-observed events. With significant differences among the NIR light-curves of SNe Ia with similar $\Delta m_{15}(B)$ values, though, template fitting in $iYJH$ based on the $\Delta m_{15}(B)$ parameter alone may be subject to significant uncertainties. Here, we proceed to cautiously apply templates when needed, while using the BF subsample of objects, for which no template-fitting is needed, to check our results.

3. Investigating the Homogeneity of Peak Luminosity of SNe Ia in the NIR

3.1. Distance Moduli, Color Excess, and Reddening

In this section we use our homogenous sample of light-curves to examine the precision of SNe Ia as standard candles in the NIR bands. We calibrate the absolute magnitudes of our objects using a technique first proposed by Phillips et al. (1999), which examines the corre-

lation between reddening-corrected, absolute peak magnitudes vs. decline-rate according to the model:

$$\mu_X = m_X - M_X(0) - b_X[\Delta m_{15}(B) - 1.1] - R_X E(B - V), \quad (1)$$

where μ_X is the distance modulus, m_X is the peak apparent magnitude corrected for Galactic reddening given in band X , $M_X(0)$ is the peak absolute magnitude for $\Delta m_{15}(B)=1.1$ and zero color excess, b_X is the slope of the luminosity vs. decline-rate relation, R_X is the total-to-selective absorption coefficient given in band X , and $E(B-V)$ is the SN color excess due to host-galaxy dust.

To calculate the distance modulus, which is used to transform rest-frame apparent magnitude to absolute magnitude, we employ the following approximation to the luminosity distance:

$$d_L(z_{CMB}; H_0, \Omega_M, \Omega_\Lambda) = \frac{(1 + z_{helio})}{(1 + z_{CMB})} \frac{c}{H_0} \left[z_{CMB} + \frac{1}{2} \left(\Omega_\Lambda - \frac{\Omega_M}{2} + 1 \right) z_{CMB}^2 \right], \quad (2)$$

where z_{helio} is the heliocentric redshift of the host-galaxy; z_{CMB} is the redshift of the host-galaxy in the cosmic microwave background (CMB) rest frame; and the standard cosmological parameters are $H_0 = 72 \text{ km s}^{-1} \text{ Mpc}^{-1}$ (Freedman et al. 2001), $\Omega_M = 0.28$, and $\Omega_\Lambda = 0.72$ (Spergel et al. 2007). Values of z_{helio} and z_{CMB} are given in Table 1. The uncertainty in the velocity of the host-galaxies due to peculiar velocity is assumed to be $\sigma_z=0.001$ (300 km s^{-1}).

For SNe that are not in the smooth Hubble flow (i.e., $z \lesssim 0.01$), distances derived using equation (2) can be inaccurate. Seven of our objects fall into this category: SNe 2005am, 2005ke, 2006D, 2006X, 2006mr, 2007af, and 2007on. Four of these (SNe 2005ke, 2006X, 2006mr, and 2007on) have published Cepheid or surface brightness fluctuation distances for their host-galaxies, which were used (see Table 2); the other three objects were excluded from our sample, leaving a sample of 24 SNe Ia.

For our complete sample, we employ a mix of cubic-spline (when peak is observed) and template (when necessary) fits to the light-curves to derive the parameters of m^{max} and $\Delta m_{15}(B)$. Table 1 lists the fitting method for each SN Ia, and Table 3 lists the K -corrected spline and template-derived apparent peak magnitude in $BVYJH$ for each object. K -corrections are applied to convert the observed magnitudes to rest-frame magnitudes using the Hsiao et al. (2007) spectral templates. For further details on the K -correction procedure, see Burns et al. (2011).

All peak magnitudes have been corrected for Galactic reddening using the values $E(B - V)_{gal}$ given in Table 1 (Schlegel et al. 1998) and adopting $R_V^{Gal}=3.1$ (a further discussion on this

point follows). In order to estimate extinction in the host-galaxies, we have used color excesses $E(B - V)$ obtained from the observed SNe colors as follows. For SNe with $\Delta m_{15}(B) < 1.7$, the host-galaxy color excesses in column (7) of Table 1 are derived using the intrinsic $B_{max}-V_{max}$ color law at maximum light derived by Folatelli et al. (2010). The Folatelli et al. relation is only valid for $\Delta m_{15}(B) < 1.7$; therefore, to calculate $E(B-V)_{host}$ for the three fast-declining events, the re-derived CSP Lira law (1995) described by Folatelli et al. (2010) is used. We do not apply any priors to the color excess measurements; therefore, negative reddenings are possible and, indeed, expected due to the measurement uncertainty and intrinsic color dispersion in SNe Ia.

Significant debate exists on the “best” value of the total-to-selective absorption coefficient for the host-galaxy, R_V , for SNe Ia studies. By reducing the scatter in the Hubble diagram, some studies (e.g., Tripp & Branch 1999; Wang et al. 2006; Astier et al. 2006; Elias-Rosa et al. 2006; Conley et al. 2007; Nobili & Goobar 2008) find that SNe Ia “prefer” a lower R_V value ($R_V=1.0-2.4$) compared with the value obtained through typical lines of sight in the Milky Way ($R_V=3.1$). Other studies (Wang et al. 2009; Folatelli et al. 2010; Foley & Kasen 2011; Mandel et al. 2010) that examine the colors of SNe Ia as a function of wavelength find that the choice between a high or low R_V value depends on the reddening of the particular SN. It appears that SNe Ia that suffer from minimal–to–moderate extinction tend to favor a value close to $R_V=3.1$, while those that suffer from high extinction favor a lower value. These studies conclude that the low derived R_V values are, in all likelihood, *not* physically due to changes in the actual reddening coefficient, but rather to some as yet-unknown parameter affecting the intrinsic color of SN Ia light-curves (see, however, Wang et al. 2009).

The reason for these differing R_V values is not well understood, and the exact value depends on the method used to derive it. Given our specific goal of removing the effects of dust extinction from SN Ia light-curves in the most accurate (i.e., physically understood) manner possible, we choose to use the typical Galactic value of $R_V=3.1$. We emphasize that our primary purpose in this study is to examine the dependence of intrinsic (i.e., corrected only for extrinsic effects, such as dust extinction) peak absolute magnitude on decline-rate in the NIR bands – not to minimize dispersion in the Hubble diagram or to calculate cosmological parameters; thus, choosing $R_V=3.1$ is warranted. As we shall see, since the effects of dust extinction in the NIR are minimal, this choice is not crucial for the results obtained. Indeed, as pointed out by Krisciunas et al. (2000) and Folatelli et al. (2010), this is one of the significant advantages of working in the NIR.

3.2. Luminosity Versus Decline-Rate Relation

In this section we investigate the correlation between peak luminosity and decline-rate for 5 different subsamples (see Table 4). We investigate the 5 subsamples in order to isolate the possible systematic effects that individual SNe Ia may have on the fit. Since each R_X (being a function only of R_V) is fixed, we solve only for $M_X(0)$ and b_X using equation (1) in the following analyses.

Subsample 1. Includes all 24 SNe Ia (i.e., the complete sample of 27 SNe Ia minus the three for which distances are not available [see §3.1]). As shown in Table 5 and displayed in Figure 5, all three of the NIR bands show a statistically significant luminosity vs. decline-rate correlation, with a dependence in all three NIR bands comparable with those in the B -band found by Prieto et al. (2006). However, as seen from the next subsample, the fast-declining and highly reddened objects have a very large effect on the derived slope.

Subsample 2. Excludes the three fast-declining SNe Ia and the two most highly reddened objects (SNe 2005A and 2006X). The highly reddened objects were excluded in order to minimize the systematic uncertainties due to the apparent peculiar nature of the reddening that affects them (Folatelli et al. 2010). We choose to remove the SNe Ia with $\Delta m_{15}(B) > 1.7$ because this decline-rate cutoff is widely used in other peak luminosity vs. decline-rate studies (Hamuy et al. 1996a; Phillips et al. 1999; Krisciunas 2004a,c; Prieto et al. 2006; Folatelli et al. 2010), and as found by Krisciunas et al. (2009), such objects appear to obey a different peak luminosity vs. decline-rate relation compared with normal SNe Ia and should therefore be modeled separately. Omitting the highly reddened and fast-declining events creates a shallower slope on the luminosity vs. decline-rate relation compared with subsample 1 for all three NIR bands (Fig. 6), with the rms dispersion decreasing significantly in all bands as well. There is evidence for a weak correlation between peak luminosity and decline-rate in Y , with the significance of the measured slope being 1.5σ , and a strong correlation in both J and H at the 3σ significance level.

Subsample 3. Uses SNe Ia, with first observations starting within 5 days after NIR peak brightness. This subsample also omits the highly reddened and fast-declining events. Like subsample 2, the Y -band shows a marginal (1.7σ) dependence of absolute peak magnitude on decline-rate, while both the J - and H -bands show a stronger (2.8σ) correlation between peak absolute magnitude and decline-rate (see Table 5 and Fig. 7). As shown in Figure 7 and Table 5, the rms scatter decreases significantly in YJH , compared with subsample 2.

Subsample 4. Uses the BF subsample, which ensures that purely empirical values for the peak magnitude and $\Delta m_{15}(B)$ are used, and avoids the unknown systematics that plague

the template fitting process. This set produces the largest peak luminosity vs. decline-rate dependence of any set examined (see Fig. 8 and Table 5), but as shown by subsample 5, this is likely due to the inclusion of the highly reddened SN 2006X and the three fast-declining events.

Subsample 5. Same as subsample 4, but excludes the highly reddened SN 2006X and the fast-declining [$\Delta m_{15}(B) > 1.7$] SNe Ia. This subsample has 7 objects with a maximum $\Delta m_{15}(B)$ of 1.39. For this restricted sample, there appears to be only little dependence of peak luminosity on decline-rate within the uncertainties for the Y - and J -bands. The calculated slopes are 0.14 ± 0.47 and 0.31 ± 0.26 for Y and J , respectively. In H , there is a marginal (2σ) detection of a correlation between peak luminosity and decline-rate (see Fig. 9). These results are consistent with the luminosity vs. decline-rate relations derived from subsamples 2 and 3. The scatter on the corrected magnitudes range between 0.05–0.14 mag, with the smallest dispersion in H and the largest in Y .

3.3. Comparison with Previous Studies

To test whether corrections for decline-rate substantially improve the precision with which SNe Ia can be used as standardizable candles in the NIR, one can examine the dispersion in derived absolute magnitude before and after such corrections are applied. From examination of Table 6, which displays both the uncorrected ($b_X = 0$) and corrected rms values given an $R_V = 3.1$ for the 5 subsamples used throughout the article, we find that a significant rms decrease occurs for the H -band, followed by the J -band. The degree of confidence for a non-zero slope in each bandpass [i.e., that a relationship exists between $\Delta m_{15}(B)$ and absolute brightness] is indicated in column (6) of Table 6. Using the t-test statistic, and based on the degrees of freedom for the fit, the confidence level for a non-zero slope was calculated. For all but subsample 5, we can exclude a zero slope at the 93% confidence level or better. This decrease in the rms and the high confidence levels confirm our earlier findings that correcting observed SNe Ia values in the J - and H -bands may substantially improve their utility as cosmological distance indicators.

To compare with previous studies, we focus on the uncorrected dispersion in Table 6 for subsample 2. We note that the intrinsic (i.e., uncorrected) dispersions found for subsample 2 (0.16 mag and 0.17 mag for J and H , respectively) compare well with the rms values of Krisciunas et al. (2009) for SNe Ia whose NIR light-curves peak before the epoch of B_{max} (0.16 mag in J and 0.15 mag in H) and of Wood-Vasey et al. (2008) in H (0.15 mag). Our J -band rms value is much less than the J -band rms value of 0.33 mag found by Wood-Vasey et al. (2008).

3.4. The Effect of R_V on Derived Correlations

Given that the value for R_V is a hot topic of debate in SNe Ia studies, we examine the effect that lowering R_V (from $R_V=3.1$ to $R_V=1.7$) has on the slope of the peak absolute YJH magnitudes vs. decline-rate relation. The same five subsamples described in §3.2 are used for this investigation. The measured slopes are given in the first two rows for each filter and subsample in Table 6.

The derived slopes for the two R_V values in subsample 1 are within the measured uncertainties for each NIR band. Subsample 2 produces the smallest variance between slopes, given different values of R_V . Subsamples 3 and 4 show a larger deviation between slopes in all three NIR bands, but all slopes are within measured uncertainties. The derived slopes for subsample 5 show a smaller variance than subsamples 1, 3, and 4. For all five subsamples, the slopes are rather insensitive to the exact value of R_V .

3.5. Hubble Diagram

Using the distance modulus derived from equation (1) and the CMB redshifts taken from NASA/IPAC Extragalactic Database (NED), we construct a Hubble diagram, which is plotted in Figure 10. We use SNe and fit parameters from subsample 2 to derive the distance modulus for each SN in YJH and B -bands [$M_B(0) = -19.222(005)$, $b_B = 1.042(213)$]. The distance moduli for the three NIR bands are averaged for each object. The resulting Hubble diagram for the combined NIR bands and B -band is shown in the top panel of Figure 10. The solid line represents the adopted concordance model of equation (2). The residuals between the corrected distance modulus and the standard cosmology are shown in the bottom panels of Figure 10. We find a combined rms scatter of 0.13 mag, or 6% in distance, for the NIR bands and a rms scatter of 0.22 mag, or 11% in distance, for the B -band. The decrease in scatter from optical bands to NIR bands on the Hubble diagram provides strong evidence that SNe Ia in NIR bands are excellent standard candles.

Note that the dispersion of 0.13 mag obtained in the NIR includes the effects of peculiar velocities. This was demonstrated by Folatelli et al. (2010), who pointed out that the residuals in the Hubble diagram in separate filters are highly correlated. Peculiar velocities also explain why the dispersion in Figure 10 decreases with redshift. Hence, the true precision of SNe Ia as distance indicators in the NIR is almost certainly better than 6%.

4. Bimodal Distribution of Absolute Magnitudes for Fast-Declining SNe Ia

Figures 5 and 8 indicate a range of peak luminosities for the fast-declining SNe Ia. Krisciunas et al. (2009) suggest that, instead of a range of peak brightnesses, there is a bimodal distribution of peak absolute NIR magnitudes for the fast-declining objects; those with NIR maximum occurring after the time of B -band maximum (t_B^{max}) are subluminous and those with NIR maximum occurring prior to t_B^{max} have standard brightnesses compared with “normal” SNe Ia. Our data are consistent with this bimodal distribution hypothesis. Our sample has three fast-declining SNe Ia: SN 2005ke ($\Delta m_{15}(B) = 1.75$), SN 2006mr ($\Delta m_{15}(B)=1.81$), and SN 2007on ($\Delta m_{15}(B)=1.89$). As shown in Table 7, SNe 2005ke and 2006mr have an average NIR maxima that occurs ~ 2 -4 days after t_B^{max} and are, on average, 0.89 mag fainter in M_Y , 0.98 mag fainter in M_J , and 0.63 mag fainter in M_H than the average peak luminosity of the slow to midrange-decliners, respectively, whereas SN 2007on has NIR maximum that occurs ~ 2 days prior to t_B^{max} and has standard peak absolute brightness in all three NIR bands. It is not surprising that this same bimodality in the absolute magnitude found by Krisciunas et al. (2009) is also found in our sample seeing, as our sample contains some of the same objects that were used in the Krisciunas et al. (2009) study. It was also found by Krisciunas et al. (2009) that fast-decliners with standard brightnesses, such as SN 2007on, show a distinct secondary maxima in the NIR, much like slow-declining objects, whereas the subluminous fast-decliners have monotonically declining light-curves in all bands. Our three fast-declining objects show this trend (see Figure 2).

We re-examine the peak absolute magnitude vs. decline-rate relationship, excluding the two subluminous fast-decliners and including the standard fast-decliner. Subsamples 2 and 5 described in §3.2 are used for this analysis, SNe 2005ke and 2006mr are omitted and SN 2007on is included for each subsample. The fit parameters derived are given in Table 8.

Including SN 2007on and excluding the two subluminous fast-decliners creates no significant change in slopes for the three NIR bands in subsamples 2 and 5, with the significance on the measured slopes remaining the same. The only case where the fiducial absolute peak magnitude significantly changes when SN 2007on is included is for the J -band in subsample 2. The absolute peak magnitudes for the other bands in subsamples 2 and 5 change very little. Our findings here confirm the Krisciunas et al. (2009) results that SNe Ia with NIR maximum occurring prior to B -band maximum, such as SN 2007on, have absolute peak magnitudes that are consistent with the absolute peak magnitudes of slow- to mid-decliners, allowing these SNe Ia to be used for the peak absolute magnitude vs. decline-rate relationship analysis.

5. Discussion and Conclusion

We analyze 27 of the best-observed SNe Ia from the first 4 years of the CSP. Spline curves were fit to the 13 objects with observed maxima in YJH . A “training set” was created from these 13 SNe Ia to construct light-curve templates for the other 14 objects with no observed NIR maxima. Light-curve properties obtained from these fits were used to calculate peak absolute magnitude, and correlations were sought with B -band decline-rates.

We discuss difficulties encountered when fitting templates to the NIR light-curves, due to the variations in the strength of the secondary maximum at a given decline-rate. The problems are especially pronounced for fast-decliners; however, if the observations begin within 5 days after NIR maximum, SNooPy provides peak magnitudes with an accuracy of ~ 0.04 mag. Obtaining additional SNe Ia light-curves with observed NIR maxima would be ideal, since splines can be directly fit, but this poses an observational challenge, since NIR maximum typically occurs several days earlier than it does in optical bands. Finding a second light-curve parameter [i.e., other than $\Delta m_{15}(B)$] could certainly be beneficial when fitting NIR light-curve templates to data; our limited sample size, however, makes such an investigation problematic. Future larger samples of SNe Ia observed in the NIR could possibly provide evidence for this second parameter and increase the accuracy of fitting templates to NIR light-curves, regardless of when the observations begin.

From our original sample of 27 objects, we examine whether a “Phillips relation” exists for the observed data that improves the standardizability of SNe Ia in the NIR for five different subsamples. R_V was kept fixed at 3.1, although the results are shown to not change appreciably if lower values are used. Consistent with earlier findings, we find that any peak luminosity vs. decline-rate dependence does indeed decrease in the NIR compared with the optical, confirming that SNe Ia are better “standard candles” at longer wavelengths.

When fast-decliners and highly reddened events are removed from the sample (e.g., subsample 2), a weaker dependence of absolute peak magnitude on decline-rate is found, with the significance of the measured slope being 1.5σ for the Y -band and 3σ for the J - and H -bands. The fact that the rms dispersion decreases significantly when the fast-declining SNe Ia are removed confirms the finding by Krisciunas et al. (2009) that a simple linear relationship cannot be used to fit both the slow- to midrange-decliners and the fast-decliners. For subsample 3, which uses SNe Ia whose first observations begin within 5 days after NIR maxima, we find a weak (1.7σ) dependence of Y peak luminosity on decline-rate and a stronger (2.8σ) dependence of J - and H -peak luminosities on decline-rate. The dispersion decreases significantly for subsample 3, compared with subsample 2. Subsample 4, which uses the BF subsample, shows the largest correlation between peak absolute magnitude and decline-rate, but the fast-declining SNe Ia strongly affect the slope. For subsample 5, which

uses the BF subsample excluding the fast-decliners and the highly reddened object, there is no significant dependence of peak Y luminosity on decline-rate. There appears to be a weak (1.2σ) correlation between decline-rate and the J -band absolute peak magnitude in subsample 5 and still a marginal (2.0σ) correlation between decline-rate and absolute peak magnitude in H . After removal of the highly reddened and fast-declining SNe Ia, we find evidence at the 2.0 - 3.0σ level for a luminosity vs. decline-rate relations in J and H , but minimal evidence for such a relation in Y .

The lowest dispersions in the uncorrected absolute magnitudes are obtained when the highly reddened and fast-declining SNe Ia are removed from the sample. Comparing the uncorrected and corrected values, we are at least 93% confident that the slope is nonzero for subsamples 1-4. It could be beneficial to correct the peak luminosity in both the J - and H -bands in order for SNe Ia to be utilized as precise standard candles in the NIR. The dispersions obtained are smaller than those found in previous NIR studies.

As larger samples of SNe Ia in the NIR are gathered, and especially as more objects are observed pre-maximum in the NIR, an interesting study could be to investigate whether using a Δm_{15} -like relation, defined in the NIR bands (rather than in the B -band) would further decrease the dependence of absolute peak magnitude on decline-rate. Our sample presented here does not include enough objects that have observed NIR maxima to test this idea, but future SNe Ia studies will certainly have more observations that cover the NIR peak with greater frequency.

Evidence for a bimodal distribution was found for the NIR absolute peak magnitudes of our fast-declining SNe Ia. The SN from our sample that peaked before the time of B -band maximum (SN 2007on) had a “normal” peak luminosity, whereas those that peaked after the time of B -band maximum (SNe 2005ke and 2006mr) had subluminous absolute peak magnitudes compared with the rest of the sample. It will be interesting to see if future SNe Ia studies find any slow- to midrange-decliners that possess this bimodal distribution. It would also be beneficial to obtain larger samples of the fast-declining SNe Ia at NIR, in addition to optical passbands, to further our understanding of these “peculiar” SNe Ia.

We also present a Hubble diagram for the NIR bands and the B -band, using the parameters derived from subsample 2. The rms scatter greatly decreases going from optical to NIR bands (0.22 mag in B to 0.13 mag for combined NIR bands), again demonstrating that SNe Ia observed in NIR bands are excellent standard candles. The Hubble diagram and Hubble residuals in Figure 10, along with the weaker dependence of absolute peak magnitude on decline-rate found for the NIR bands compared with the optical bands, clearly show the advantages of working in the NIR for distance determinations and cosmological studies. Future high- z SNe Ia cosmological studies may therefore benefit from observations taken in the

rest-frame NIR bands, since SNe Ia appear to be better standard candles in these passbands than in the optical (i.e., they have a weaker dependence of absolute NIR peak magnitude on decline-rate, systematic uncertainties are minimized due to the reduced effects of dust extinction, and NIR passbands are relatively insensitive to the exact value of R_V used). The Y -band, in particular, appears to hold significant promise for such future studies, since it offers an optimal combination of signal-to-noise ratio, low sensitivity to dust extinction, and an essentially negligible dependence of absolute peak magnitude on decline-rate.

The authors extend their special thanks to Luis Boldt, Carlos Contreras, Sergio Gonzalez, Wojtek Krzeminski, and Francisco Salgado, who worked very hard to gather and reduce the data that are analyzed in this article. This work is supported by the National Science Foundation (NSF) under grants AST-0306969, AST-0607438, and AST-1008343. Support for research on the extragalactic distance scale at San Diego State University is provided by proposal number AR-10673, provided by NASA through a grant from the Space Telescope Science Institute, which is operated by the Association of Universities for Research in Astronomy, Inc., under NASA contract NAS5-26555. DCL and SK also acknowledge support from NSF grant AST-1009571. M.H. acknowledges support from the Millennium Center for Supernova Science through grant P10-064-F from Iniciativa Científica Milenio, Centro de Astrofísica FONDAF 15010003, and Center of Excellence in Astrophysics and Associated Technologies (PFB 06). G.F. acknowledges support from FONDECYT grant 3090004.

REFERENCES

- Ajhar, E. A., Tonry, J. L., Blakeslee, J. P., Riess, A. G., & Schmidt, B. P. 2001, *ApJ*, 559, 584
- Astier, P., et al. 2006, *A&A*, 447, 31
- Blondin, S., Mandel, K. S., & Kirshner, R. P. 2011, *A&A*, 526, A81
- Burns, C. R., et al. 2011, *AJ*, 141, 19
- Cardelli, J. A., Clayton, G. C., & Mathis, J. S. 1989, *ApJ*, 345, 245
- Conley, A., Carlberg, R. G., Guy, J., Howell, D. A., Jha, S., Riess, A. G., & Sullivan, M. 2007, *ApJ*, 664, L13
- Conley, A., et al. 2008, *ApJ*, 681, 482
- Contreras, C., et al. 2010, *AJ*, 139, 519

- Elias, J. H., Frogel, J. A., Hackwell, J. A., & Persson, S. E. 1981, *ApJ*, 251, L13
- Elias, J. H., Matthews, K., Neugebauer, G., & Persson, S. E. 1985, *ApJ*, 296, 379
- Elias-Rosa, N., et al. 2006, *MNRAS*, 369, 1880
- Folatelli, G., et al. 2010, *AJ*, 139, 120
- Foley, R. J., & Kasen, D. 2011, *ApJ*, 729, 55
- Freedman, W. L., et al. 2001, *ApJ*, 553, 47
- Freedman, W. L., et al. 2009, *ApJ*, 704, 1036
- Frogel, J. A., Gregory, B., Kawara, K., Laney, D., Phillips, M. M., Terndrup, D., Vrba, F., & Whitford, A. E. 1987, *ApJ*, 315, L129
- Gallagher, J. S., Garnavich, P. M., Caldwell, N., Kirshner, R. P., Jha, S. W., Li, W., Ganeshalingam, M., & Filippenko, A. V. 2008, *ApJ*, 685, 752
- Goldhaber, G., et al. 2001, *ApJ*, 558, 359
- Guy, J., Astier, P., Nobili, S., Regnault, N., & Pain, R. 2005, *A&A*, 443, 781
- Guy, J., et al. 2007, *A&A*, 466, 11
- Hamuy, M., Phillips, M. M., Suntzeff, N. B., Schommer, R. A., Maza, J., & Aviles, R. 1996, *AJ*, 112, 2391
- Hamuy, M., et al. 2006, *PASP*, 118, 2
- Hsiao, E. Y., Conley, A., Howell, D. A., Sullivan, M., Pritchett, C. J., Carlberg, R. G., Nugent, P. E., & Phillips, M. M. 2007, *ApJ*, 663, 1187
- Jensen, J. B., Tonry, J. L., Barris, B. J., Thompson, R. I., Liu, M. C., Rieke, M. J., Ajhar, E. A., & Blakeslee, J. P. 2003, *ApJ*, 583, 712
- Jha, S., et al. 1999, *ApJS*, 125, 73
- Jha, S., Riess, A. G., & Kirshner, R. P. 2007, *ApJ*, 659, 122
- Kasen, D. 2006, *ApJ*, 649, 939
- Kelly, P. L., Hicken, M., Burke, D. L., Mandel, K. S., & Kirshner, R. P. 2010, *ApJ*, 715, 743

- Kirshner, R. P., Willner, S. P., Becklin, E. E., Neugebauer, G., & Oke, J. B. 1973, *ApJ*, 180, L97
- Krisciunas, K., Hastings, N. C., Loomis, K., McMillan, R., Rest, A., Riess, A. G., & Stubbs, C. 2000, *ApJ*, 539, 658
- Krisciunas, K., Phillips, M. M., & Suntzeff, N. B. 2004a, *ApJ*, 602, L81
- Krisciunas, K., et al. 2004b, *AJ*, 127, 1664
- Krisciunas, K., et al. 2004c, *AJ*, 128, 3034
- Krisciunas, K., Prieto, J. L., Garnavich, P. M., Riley, J.-L. G., Rest, A., Stubbs, C., & McMillan, R. 2006, *AJ*, 131, 1639
- Krisciunas, K., et al. 2009, *AJ*, 138, 1584
- Lira, P. 1995, M.S. thesis, Univ. Chile (Santiago)
- Mandel, K. S., Narayan, G., & Kirshner, R. P. 2010, arXiv:1011.5910
- Meikle, W. P. S. 2000, *MNRAS*, 314, 782
- Nobili, S., & Goobar, A. 2008, *A&A*, 487, 19
- Perlmutter, S., et al. 1997, *ApJ*, 483, 565
- Persson, S. E., Madore, B. F., Krzemiński, W., Freedman, W. L., Roth, M., & Murphy, D. C. 2004, *AJ*, 128, 2239
- Phillips, M. M. 1993, *ApJ*, 413, L105
- Phillips, M. M., Lira, P., Suntzeff, N. B., Schommer, R. A., Hamuy, M., & Maza, J. 1999, *AJ*, 118, 1766
- Phillips, M. M., et al. 2003, in *Proc. ESO/MPA/WPE Workshop, From Twilight to High-light: The Physics of Supernovae* (Berlin: Springer), 193
- Prieto, J. L., Rest, A., & Suntzeff, N. B. 2006, *ApJ*, 647, 501
- Riess, A. G., Press, W. H., & Kirshner, R. P. 1996, *ApJ*, 473, 88
- Riess, A. G., et al. 1998, *AJ*, 116, 1009
- Schlegel, D. J., Finkbeiner, D. P., & Davis, M. 1998, *ApJ*, 500, 525

- Spergel, D. N., et al. 2007, ApJS, 170, 377
- Stritzinger, M., & Sollerman, J. 2007, A&A, 470, L1
- Stritzinger, M. D., Phillips, M. M., Boldt, L. N., et al. 2011, AJ, 142, 156
- Sullivan, M., et al. 2010, MNRAS, 406, 782
- Tonry, J. L., Dressler, A., Blakeslee, J. P., Ajhar, E. A., Fletcher, A. B., Luppino, G. A., Metzger, M. R., & Moore, C. B. 2001, ApJ, 546, 681
- Tripp, R., & Branch, D. 1999, ApJ, 525, 209
- Wang, X., Filippenko, A. V., Ganeshalingam, M., et al. 2009, ApJ, 699, L139
- Wang, L., Goldhaber, G., Aldering, G., & Perlmutter, S. 2003, ApJ, 590, 944
- Wang, X., Wang, L., Pain, R., Zhou, X., & Li, Z. 2006, ApJ, 645, 488
- Wood-Vasey, W. M., et al. 2008, ApJ, 689, 377

Table 1. List of Supernovae and Properties

SN	z_{helio}	z_{CMB}	$\Delta m_{15}(B)$	$E(B - V)_{gal}$	$E(B - V)_{host}$	Fit method	Subsample
(1)	(2)	(3)	(4)	(5)	(6)	(7)	(8)
2004ef	0.0310	0.029	1.345(017)	0.056(006)	0.097(008)	Template	1, 2, 3
2004eo	0.0157	0.0147	1.370(055)	0.108(011)	0.014(018)	Spline	1, 2, 3, 4, 5
2004ey	0.0158	0.0146	0.935(014)	0.139(014)	-0.052(005)	Template	1, 2, 3
2004gs	0.0267	0.0275	1.502(016)	0.031(003)	0.157(005)	Template	1, 2
2004gu	0.0459	0.0469	0.900(045)	0.026(003)	0.183(009)	Template	1, 2, 3
2005A	0.0191	0.0184	1.224(102)	0.030(003)	0.996(016)	Template	1
2005M	0.0220	0.0230	0.859(011)	0.031(003)	0.052(011)	Spline	1, 2, 3, 4, 5
2005ag	0.0794	0.0801	0.905(046)	0.041(004)	0.047(007)	Template	1, 2, 3
2005al	0.0124	0.0133	1.146(015)	0.055(005)	-0.094(005)	Template	1, 2, 3
2005am	0.0079	0.0090	1.509(021)	0.054(005)	-0.030(010)	Template	
2005el	0.0149	0.0149	1.345(020)	0.114(011)	-0.043(016)	Spline	1, 2, 3, 4, 5
2005eq	0.0290	0.0284	0.756(022)	0.074(007)	0.090(006)	Template	1, 2, 3
2005hc	0.0459	0.0450	0.894(014)	0.029(003)	0.048(006)	Template	1, 2, 3
2005iq	0.0340	0.0330	1.258(013)	0.022(002)	-0.040(006)	Template	1, 2, 3
2005kc	0.0151	0.0139	1.163(029)	0.132(013)	0.173(006)	Spline	1, 2, 3, 4, 5
2005ke	0.0049	0.0045	1.748(015)	0.027(003)	0.036(005)	Spline	1, , , 4
2005ki	0.0192	0.0204	1.279(038)	0.032(003)	-0.018(012)	Spline	1, 2, 3, 4, 5
2006D	0.0085	0.0097	1.388(012)	0.046(005)	0.071(010)	Spline	
2006X	0.0052	0.0063	1.107(019)	0.026(003)	1.202(013)	Spline	1
2006ax	0.0167	0.0180	0.990(016)	0.050(005)	-0.033(006)	Spline	1, 2, 3, 4, 5
2006bh	0.0109	0.0105	1.426(011)	0.026(003)	-0.038(007)	Template	1, 2, 3
2006eq	0.0495	0.0484	1.660(060)	0.048(005)	0.191(033)	Template	1, 2
2006et	0.0222	0.0212	0.903(012)	0.019(002)	0.222(008)	Spline	1, 2, 3, 4, 5
2006gt	0.0448	0.0437	1.663(037)	0.037(004)	0.165(019)	Template	1, 2
2006mr	0.0059	0.0055	1.805(015)	0.021(002)	-0.025(013)	Spline	1, , , 4
2007af	0.0055	0.0063	1.203(036)	0.039(004)	0.177(019)	Spline	
2007on	0.0065	0.0062	1.893(018)	0.011(001)	0.022(010)	Spline	1, , , 4

Note. - Col. (1) SN name; Col. (2) Heliocentric redshift from the NASA/IPAC Extragalactic Database (NED); Col. (3) Redshift in the frame of the 3K CMB (NED); Col. (4) Observed $\Delta m_{15}(B)$; Col. (5) Galactic reddening; Col. (6) Host-galaxy reddening; Col. (7) Fitting method (spline or template); Col. (8) Subsample(s) SN belongs to (see text and Table 4) If blank, SN is excluded from all subsamples.

Table 2. Derived Distance Moduli

SN	Host-galaxy	μ (mag)	Distance method	Reference
(1)	(2)	(3)	(4)	(5)
2004ef	UGC 12158	35.56 ± 0.07	LD	
2004eo	NGC 6928	34.00 ± 0.15	LD	
2004ey	UGC 11816	33.99 ± 0.15	LD	
2004gs	MCG +03–22–020	35.31 ± 0.08	LD	
2004gu	FGC 175A	36.50 ± 0.05	LD	
2005A	NGC 958	34.47 ± 0.12	LD	
2005M	NGC 2930	34.94 ± 0.10	LD	
2005ag	...	37.72 ± 0.03	LD	
2005al	NGC 5304	33.71 ± 0.16	LD	
2005am	NGC 2811	32.85 ± 0.24	LD	
2005el	NGC 1819	33.99 ± 0.14	LD	
2005eq	MCG –01–09–006	35.43 ± 0.08	LD	
2005hc	MCG +00–06–003	36.47 ± 0.05	LD	
2005iq	MCG –03–01–008	35.78 ± 0.07	LD	
2005kc	NGC 7311	33.88 ± 0.16	LD	
2005ke	NGC 1371	31.84 ± 0.08	SBF	Tonry et al. (2001)*
2005ki	NGC 3332	34.64 ± 0.11	LD	
2006D	MCG –01–33–34	33.00 ± 0.22	LD	
2006X	NGC 4321	30.91 ± 0.14	Cepheids	Freedman et al. (2001)
2006ax	NGC 3663	34.36 ± 0.12	LD	
2006bh	NGC 7329	33.23 ± 0.21	LD	
2006eq	...	36.64 ± 0.05	LD	
2006et	NGC 232	34.80 ± 0.10	LD	
2006gt	2MASX J00561810–0137327	36.41 ± 0.05	LD	
2006mr	NGC 1316	31.15 ± 0.23	SBF	Ajhar et al. (2001)
2007af	NGC 5584	32.10 ± 0.34	LD	
2007on	NGC 1404	31.45 ± 0.19	SBF	Jensen et al. (2003)

Note. - Col. (1) SN name; Col. (2) Host-galaxy; Col. (3) Distance modulus from fits of §4; Col. (4) Distance method used (LD - luminosity distance, SBF - surface brightness fluctuation); Col. (5) Reference used for SBF and Cepheid distances.

*NGC 1371 is a member of the Eridanus group/cluster. Tonry et al. (2001) give a distance modulus of 32.00 ± 0.08 mag for this group based on SBF measurements of seven members. Subtracting 0.16 mag (Jensen et al. 2003) to put this on the Freedman et al. (2001) scale gives 31.84 ± 0.08 mag.

Table 3. Supernova Light-Curve Properties

Filter	t_{max} (JD $-2,453,000$) (days)	m_{max} (spline) (mag)	m_{max} (template) (mag)
(1)	(2)	(3)	(4)
SN 2004ef			
<i>B</i>	264.40 ± 0.05	...	17.077 ± 0.007
<i>V</i>	265.88 ± 0.05	...	16.910 ± 0.004
<i>Y</i>	261.47 ± 0.05	...	16.999 ± 0.008
<i>J</i>	261.44 ± 0.05	...	17.020 ± 0.114
<i>H</i>	261.04 ± 0.05	...	17.409 ± 0.027
SN 2004eo			
<i>B</i>	278.69 ± 0.28	15.497 ± 0.013	15.552 ± 0.011
<i>V</i>	280.68 ± 0.54	15.359 ± 0.012	15.346 ± 0.006
<i>Y</i>	275.85 ± 0.91	15.929 ± 0.102	15.863 ± 0.027
<i>J</i>	274.85 ± 0.19	15.547 ± 0.010	15.515 ± 0.025
<i>H</i>	274.18 ± 0.13	15.814 ± 0.010	15.742 ± 0.024
SN 2004ey			
<i>B</i>	304.87 ± 0.04	...	15.275 ± 0.004
<i>V</i>	306.20 ± 0.04	...	15.224 ± 0.003
<i>Y</i>	300.61 ± 0.04	...	15.747 ± 0.033
<i>J</i>	301.40 ± 0.04	...	15.540 ± 0.021
<i>H</i>	300.88 ± 0.04	...	15.757 ± 0.018
SN 2004gs			
<i>B</i>	356.23 ± 0.07	...	17.277 ± 0.003
<i>V</i>	357.92 ± 0.07	...	17.057 ± 0.004
<i>Y</i>	353.77 ± 0.07	...	17.241 ± 0.022
<i>J</i>	353.81 ± 0.07	...	17.138 ± 0.032
<i>H</i>	353.52 ± 0.07	...	17.236 ± 0.032
SN 2004gu			
<i>B</i>	362.56 ± 0.20	...	17.570 ± 0.007
<i>V</i>	363.91 ± 0.20	...	17.401 ± 0.005
<i>Y</i>	357.98 ± 0.20	...	17.991 ± 0.046

Table 3—Continued

Filter	t_{max} (JD $-2,453,000$) (days)	m_{max} (spline) (mag)	m_{max} (template) (mag)
(1)	(2)	(3)	(4)
<i>J</i>	359.01 ± 0.20	...	17.934 ± 0.093
<i>H</i>	358.28 ± 0.20	...	18.103 ± 0.050
SN 2005A			
<i>B</i>	378.86 ± 0.24	...	18.239 ± 0.013
<i>V</i>	380.18 ± 0.24	...	17.214 ± 0.010
<i>Y</i>	374.59 ± 0.24	...	16.306 ± 0.022
<i>J</i>	375.37 ± 0.24	...	16.129 ± 0.023
<i>H</i>	374.85 ± 0.24	...	16.302 ± 0.022
SN 2005M			
<i>B</i>	406.02 ± 0.20	16.041 ± 0.004	16.048 ± 0.003
<i>V</i>	407.49 ± 0.12	16.003 ± 0.010	15.998 ± 0.002
<i>Y</i>	402.52 ± 0.81	16.627 ± 0.036	16.587 ± 0.006
<i>J</i>	402.59 ± 0.94	16.459 ± 0.046	16.463 ± 0.013
<i>H</i>	401.38 ± 0.06	16.458 ± 0.074	16.652 ± 0.010
SN 2005ag			
<i>B</i>	414.79 ± 0.14	...	18.607 ± 0.005
<i>V</i>	416.22 ± 0.14	...	18.558 ± 0.005
<i>Y</i>	410.17 ± 0.14	...	19.325 ± 0.032
<i>J</i>	411.10 ± 0.14	...	19.244 ± 0.048
<i>H</i>	410.53 ± 0.14	...	19.044 ± 0.063
SN 2005al			
<i>B</i>	429.86 ± 0.13	...	15.045 ± 0.003
<i>V</i>	431.11 ± 0.13	...	15.094 ± 0.004
<i>Y</i>	426.42 ± 0.13	...	15.576 ± 0.035
<i>J</i>	426.55 ± 0.13	...	15.355 ± 0.048
<i>H</i>	426.04 ± 0.13	...	15.706 ± 0.021
SN 2005am			
<i>B</i>	435.90 ± 0.13	...	13.870 ± 0.008

Table 3—Continued

Filter	t_{max} (JD $-2,453,000$) (days)	m_{max} (spline) (mag)	m_{max} (template) (mag)
(1)	(2)	(3)	(4)
<i>V</i>	437.47 ± 0.13	...	13.750 ± 0.006
<i>Y</i>	433.30 ± 0.13	...	13.949 ± 0.032
<i>J</i>	433.29 ± 0.13	...	13.746 ± 0.045
<i>H</i>	432.97 ± 0.13	...	14.103 ± 0.022
SN 2005el			
<i>B</i>	647.30 ± 0.36	15.278 ± 0.011	15.307 ± 0.012
<i>V</i>	647.86 ± 0.24	15.194 ± 0.012	15.261 ± 0.005
<i>Y</i>	642.66 ± 0.15	15.559 ± 0.014	15.676 ± 0.012
<i>J</i>	643.15 ± 0.15	15.508 ± 0.008	15.574 ± 0.015
<i>H</i>	642.33 ± 0.12	15.652 ± 0.010	15.697 ± 0.012
SN 2005eq			
<i>B</i>	654.60 ± 0.10	...	16.565 ± 0.004
<i>V</i>	655.93 ± 0.10	...	16.458 ± 0.004
<i>Y</i>	650.09 ± 0.10	...	17.062 ± 0.020
<i>J</i>	651.11 ± 0.10	...	16.868 ± 0.019
<i>H</i>	650.39 ± 0.10	...	17.122 ± 0.022
SN 2005hc			
<i>B</i>	667.71 ± 0.07	...	17.431 ± 0.004
<i>V</i>	669.10 ± 0.07	...	17.395 ± 0.004
<i>Y</i>	663.18 ± 0.07	...	18.049 ± 0.025
<i>J</i>	664.14 ± 0.07	...	17.922 ± 0.026
<i>H</i>	663.55 ± 0.07	...	18.003 ± 0.051
SN 2005iq			
<i>B</i>	688.03 ± 0.05	...	16.887 ± 0.004
<i>V</i>	689.29 ± 0.05	...	16.902 ± 0.004
<i>Y</i>	684.42 ± 0.05	...	17.442 ± 0.021
<i>J</i>	684.61 ± 0.05	...	17.365 ± 0.016
<i>H</i>	684.08 ± 0.05	...	17.513 ± 0.025

Table 3—Continued

Filter	t_{max} (JD $-2,453,000$) (days)	m_{max} (spline) (mag)	m_{max} (template) (mag)
(1)	(2)	(3)	(4)
SN 2005kc			
<i>B</i>	698.29 ± 0.22	16.037 ± 0.004	16.063 ± 0.012
<i>V</i>	699.19 ± 0.08	15.744 ± 0.004	15.745 ± 0.006
<i>Y</i>	693.97 ± 0.17	15.658 ± 0.014	15.626 ± 0.014
<i>J</i>	694.69 ± 0.73	15.479 ± 0.010	15.455 ± 0.016
<i>H</i>	694.10 ± 0.55	15.684 ± 0.013	16.644 ± 0.010
SN 2005ke			
<i>B</i>	698.81 ± 0.07	14.882 ± 0.006	14.890 ± 0.013
<i>V</i>	701.32 ± 0.24	14.189 ± 0.005	14.202 ± 0.018
<i>Y</i>	701.26 ± 0.70	14.055 ± 0.018	14.078 ± 0.008
<i>J</i>	700.15 ± 0.10	14.048 ± 0.006	14.016 ± 0.010
<i>H</i>	702.07 ± 0.13	13.932 ± 0.008	13.928 ± 0.004
SN 2005ki			
<i>B</i>	706.13 ± 1.28	15.689 ± 0.011	15.690 ± 0.009
<i>V</i>	706.40 ± 0.19	15.670 ± 0.005	15.698 ± 0.007
<i>Y</i>	701.62 ± 0.06	16.233 ± 0.011	16.278 ± 0.012
<i>J</i>	702.73 ± 0.26	16.129 ± 0.012	16.186 ± 0.020
<i>H</i>	701.48 ± 0.75	16.265 ± 0.028	16.321 ± 0.024
SN 2006D			
<i>B</i>	757.75 ± 0.06	14.319 ± 0.007	14.339 ± 0.008
<i>V</i>	759.13 ± 0.19	14.183 ± 0.007	14.212 ± 0.004
<i>Y</i>	754.85 ± 0.05	14.754 ± 0.117	14.630 ± 0.013
<i>J</i>	755.05 ± 0.067	14.379 ± 0.008	14.460 ± 0.010
<i>H</i>	754.90 ± 0.055	14.500 ± 0.007	14.590 ± 0.008
SN 2006X			
<i>B</i>	786.23 ± 0.14	15.324 ± 0.007	15.383 ± 0.021
<i>V</i>	789.18 ± 0.13	14.111 ± 0.011	14.111 ± 0.010
<i>Y</i>	781.50 ± 0.11	13.144 ± 0.007	13.175 ± 0.017

Table 3—Continued

Filter	t_{max} (JD $-2,453,000$) (days)	m_{max} (spline) (mag)	m_{max} (template) (mag)
(1)	(2)	(3)	(4)
<i>J</i>	782.74 ± 0.12	12.866 ± 0.006	12.901 ± 0.012
<i>H</i>	781.76 ± 0.12	12.996 ± 0.004	12.999 ± 0.010
SN 2006ax			
<i>B</i>	827.59 ± 0.13	15.201 ± 0.005	15.213 ± 0.007
<i>V</i>	828.27 ± 0.36	15.211 ± 0.002	15.228 ± 0.005
<i>Y</i>	823.47 ± 0.57	15.835 ± 0.012	15.932 ± 0.014
<i>J</i>	823.72 ± 0.55	15.740 ± 0.011	15.754 ± 0.012
<i>H</i>	824.24 ± 0.40	15.922 ± 0.021	16.046 ± 0.010
SN 2006bh			
<i>B</i>	833.65 ± 0.04	...	14.488 ± 0.006
<i>V</i>	835.00 ± 0.04	...	14.477 ± 0.004
<i>Y</i>	830.57 ± 0.04	...	14.978 ± 0.009
<i>J</i>	830.57 ± 0.04	...	14.930 ± 0.018
<i>H</i>	830.13 ± 0.04	...	15.043 ± 0.014
SN 2006eq			
<i>B</i>	976.72 ± 0.43	...	18.726 ± 0.027
<i>V</i>	978.73 ± 0.43	...	18.438 ± 0.019
<i>Y</i>	975.28 ± 0.43	...	18.236 ± 0.018
<i>J</i>	975.60 ± 0.43	...	18.247 ± 0.114
<i>H</i>	975.55 ± 0.43	...	18.374 ± 0.065
SN 2006et			
<i>B</i>	993.55 ± 0.37	16.038 ± 0.004	16.060 ± 0.007
<i>V</i>	995.75 ± 0.21	15.859 ± 0.008	15.865 ± 0.004
<i>Y</i>	989.27 ± 1.07	16.344 ± 0.016	16.333 ± 0.013
<i>J</i>	990.48 ± 0.53	16.055 ± 0.063	16.113 ± 0.012
<i>H</i>	989.34 ± 0.27	16.323 ± 0.031	16.401 ± 0.019
SN 2006gt			
<i>B</i>	1003.15 ± 0.10	...	18.383 ± 0.016

Table 3—Continued

Filter	t_{max} (JD $-2,453,000$) (days)	m_{max} (spline) (mag)	m_{max} (template) (mag)
(1)	(2)	(3)	(4)
<i>V</i>	1005.19 ± 0.10	...	18.129 ± 0.011
<i>Y</i>	1001.95 ± 0.10	...	18.326 ± 0.015
<i>J</i>	1002.28 ± 0.10	...	18.244 ± 0.034
<i>H</i>	1002.29 ± 0.10	...	18.265 ± 0.035
SN 2006mr			
<i>B</i>	1050.66 ± 0.08	15.387 ± 0.009	15.555 ± 0.019
<i>V</i>	1052.53 ± 0.04	14.640 ± 0.009	14.780 ± 0.016
<i>Y</i>	1056.68 ± 0.06	14.019 ± 0.006	14.075 ± 0.008
<i>J</i>	1054.31 ± 0.02	14.007 ± 0.004	14.107 ± 0.014
<i>H</i>	1055.30 ± 0.03	13.850 ± 0.005	13.903 ± 0.009
SN 2007af			
<i>B</i>	1174.78 ± 0.20	13.440 ± 0.011	13.450 ± 0.012
<i>V</i>	1176.16 ± 0.17	13.228 ± 0.016	13.235 ± 0.007
<i>Y</i>	1170.57 ± 0.08	13.582 ± 0.009	13.584 ± 0.007
<i>J</i>	1171.12 ± 0.04	13.469 ± 0.002	13.460 ± 0.008
<i>H</i>	1170.21 ± 0.15	13.623 ± 0.004	13.625 ± 0.005
SN 2007on			
<i>B</i>	1420.50 ± 0.08	13.085 ± 0.007	13.187 ± 0.015
<i>V</i>	1421.78 ± 0.15	12.973 ± 0.007	13.024 ± 0.009
<i>Y</i>	1418.04 ± 0.04	13.254 ± 0.005	13.388 ± 0.010
<i>J</i>	1418.68 ± 0.32	13.093 ± 0.063	13.239 ± 0.016
<i>H</i>	1418.36 ± 0.08	13.253 ± 0.006	13.285 ± 0.007

Note. - Col. (1) Filter; Col. (2) t_{max} ; Col. (3) K -corrected m_{max} spline; Col. (4) K -corrected m_{max} template.

Table 4. Description of Subsamples

Subsample	Description	N_{SNe}
1	All 24 SNe	24
2	Exc. fast-declining ($\Delta m_{15}(B) > 1.7$) and highly reddened ($E(B - V) > 0.9$)	19
3	SNe whose first observation begins ≤ 5 days after NIR maximum	
	exc. fast-declining and highly reddened events	13
4	Best fit	11
5	Best fit exc. fast-declining and highly reddened	7

Table 5. Fit Parameters of Peak NIR Magnitude Versus $\Delta m_{15}(B)$

Filter X	$M_X(0)$ (mag)	b_X (mag decline-rate $^{-1}$)	RMS (mag)	N_{SNe}	Subsample
(1)	(2)	(3)	(4)	(5)	(6)
Y	-18.535 ± 0.032	0.611 ± 0.263	0.382	24	1
J	-18.588 ± 0.028	0.691 ± 0.230	0.336	24	1
H	-18.432 ± 0.017	0.581 ± 0.153	0.235	24	1
Y	-18.494 ± 0.007	0.294 ± 0.187	0.184	19	2
J	-18.574 ± 0.003	0.363 ± 0.119	0.141	19	2
H	-18.415 ± 0.006	0.459 ± 0.140	0.142	19	2
Y	-18.461 ± 0.005	0.273 ± 0.160	0.122	13	3
J	-18.552 ± 0.002	0.392 ± 0.141	0.123	13	3
H	-18.390 ± 0.003	0.302 ± 0.109	0.086	13	3
Y	-18.598 ± 0.084	0.844 ± 0.418	0.396	11	4
J	-18.665 ± 0.092	0.878 ± 0.417	0.384	11	4
H	-18.507 ± 0.056	0.808 ± 0.276	0.250	11	4
Y	-18.505 ± 0.007	0.139 ± 0.471	0.136	7	5
J	-18.606 ± 0.003	0.307 ± 0.261	0.125	7	5
H	-18.446 ± 0.009	0.538 ± 0.273	0.053	7	5

Note. - Col. (1) Filter; Col. (2) Absolute magnitude for $\Delta m_{15}(B) = 1.1$ and no reddening; Col. (3) Luminosity vs. decline-rate slope; Col. (4) rms of fit in magnitudes; Col. (5) Number of SNe used in fits; Col. (6) Sample of SNe used in fit (see text).

Table 6. Fit Parameters

Filter	$M_X(0)$ (mag)	b_X (mag decline-rate ⁻¹)	R_V	RMS (mag)	Confidence level (%)	Subsample
(1)	(2)	(3)	(4)	(5)	(6)	(7)
<i>Y</i>	-18.418 ± 0.019	0.495 ± 0.172	1.7	0.262	99.6	1
<i>Y</i>	-18.535 ± 0.032	0.611 ± 0.263	3.1	0.382	98.4	1
<i>Y</i>	-18.530 ± 0.000	0.000	3.1	0.424	–	1
<i>J</i>	-18.490 ± 0.020	0.606 ± 0.170	1.7	0.258	99.9	1
<i>J</i>	-18.588 ± 0.028	0.691 ± 0.230	3.1	0.336	99.7	1
<i>J</i>	-18.560 ± 0.000	0.000	3.1	0.399	–	1
<i>H</i>	-18.366 ± 0.014	0.545 ± 0.131	1.7	0.201	99.9	1
<i>H</i>	-18.432 ± 0.017	0.581 ± 0.153	3.1	0.235	99.9	1
<i>H</i>	-18.389 ± 0.000	0.000	3.1	0.292	–	1
<i>Y</i>	-18.441 ± 0.005	0.413 ± 0.146	1.7	0.145	99.4	2
<i>Y</i>	-18.494 ± 0.007	0.294 ± 0.187	3.1	0.184	93.6	2
<i>Y</i>	-18.503 ± 0.000	0.000	3.1	0.189	–	2
<i>J</i>	-18.514 ± 0.002	0.376 ± 0.093	1.7	0.116	99.9	2
<i>J</i>	-18.574 ± 0.003	0.363 ± 0.119	3.1	0.141	99.6	2
<i>J</i>	-18.545 ± 0.000	0.000	3.1	0.163	–	2
<i>H</i>	-18.390 ± 0.006	0.469 ± 0.130	1.7	0.128	99.9	2
<i>H</i>	-18.415 ± 0.006	0.459 ± 0.140	3.1	0.142	99.8	2
<i>H</i>	-18.398 ± 0.000	0.000	3.1	0.169	–	2
<i>Y</i>	-18.419 ± 0.005	0.306 ± 0.115	1.7	0.098	99.0	3
<i>Y</i>	-18.461 ± 0.005	0.273 ± 0.160	3.1	0.122	94.1	3
<i>Y</i>	-18.443 ± 0.000	0.000	3.1	0.147	–	3
<i>J</i>	-18.525 ± 0.003	0.394 ± 0.113	1.7	0.101	99.7	3
<i>J</i>	-18.552 ± 0.002	0.392 ± 0.141	3.1	0.123	99.0	3

Table 6—Continued

Filter	$M_X(0)$ (mag)	b_X (mag decline-rate ⁻¹)	R_V	RMS (mag)	Confidence level (%)	Subsample
(1)	(2)	(3)	(4)	(5)	(6)	(7)
<i>J</i>	-18.544 ± 0.000	0.000	3.1	0.164	–	3
<i>H</i>	-18.371 ± 0.004	0.309 ± 0.097	1.7	0.073	99.6	3
<i>H</i>	-18.390 ± 0.003	0.302 ± 0.109	3.1	0.086	99.1	3
<i>H</i>	-18.375 ± 0.000	0.000	3.1	0.119	–	3
<i>Y</i>	-18.404 ± 0.063	0.605 ± 0.323	1.7	0.302	95.5	4
<i>Y</i>	-18.598 ± 0.084	0.844 ± 0.418	3.1	0.396	96.2	4
<i>Y</i>	-18.530 ± 0.000	0.000	3.1	0.508	–	4
<i>J</i>	-18.494 ± 0.075	0.746 ± 0.353	1.7	0.222	96.7	4
<i>J</i>	-18.665 ± 0.092	0.878 ± 0.417	3.1	0.384	96.7	4
<i>J</i>	-18.571 ± 0.000	0.000	3.1	0.516	–	4
<i>H</i>	-18.339 ± 0.050	0.591 ± 0.254	1.7	0.236	97.6	4
<i>H</i>	-18.507 ± 0.056	0.808 ± 0.276	3.1	0.250	99.1	4
<i>H</i>	-18.363 ± 0.000	0.000	3.1	0.359	–	4
<i>Y</i>	-18.464 ± 0.006	0.004 ± 0.425	1.7	0.120	–	5
<i>Y</i>	-18.505 ± 0.007	0.139 ± 0.471	3.1	0.136	–	5
<i>Y</i>	-18.507 ± 0.000	0.000	3.1	0.155	–	5
<i>J</i>	-18.591 ± 0.003	0.245 ± 0.230	1.7	0.101	83.9	5
<i>J</i>	-18.606 ± 0.005	0.307 ± 0.261	3.1	0.125	85.8	5
<i>J</i>	-18.628 ± 0.000	0.000	3.1	0.143	–	5
<i>H</i>	-18.428 ± 0.008	0.444 ± 0.270	1.7	0.054	91.5	5
<i>H</i>	-18.446 ± 0.009	0.538 ± 0.273	3.1	0.053	94.9	5
<i>H</i>	-18.442 ± 0.000	0.000	3.1	0.106	–	5

Note. - Col. (1) Filter; Col. (2) Absolute magnitude for $\Delta m_{15}(B) = 1.1$ and no reddening; Col. (3) Luminosity vs. decline-rate slope; Col. (4) Total- to-selective absorption coefficient; Col. (5) rms of fit in magnitudes; Col. (6) Percent confidence level that slope is not zero; Col. (7) Sample.

Table 7. NIR Time of Maximum and Absolute Magnitude at Maximum

Filter	t_B^{max} (days)	$\langle M \rangle$ (mag)	σ (mag)	N_{SNe}
(1)	(2)	(3)	(4)	(5)
Slow to mid-decliners				
<i>Y</i>	−3.649	−18.564	0.129	21
<i>J</i>	−3.178	−18.651	0.135	21
<i>H</i>	−3.735	−18.425	0.130	21
Early-Peaking Fast-Decliners				
<i>Y</i>	−2.500	−18.471	0.190	1
<i>J</i>	−1.820	−18.561	0.200	1
<i>H</i>	−2.140	−18.328	0.190	1
Late-Peaking Fast-Decliners				
<i>Y</i>	4.230	−17.668	0.127	2
<i>J</i>	2.490	−17.669	0.125	2
<i>H</i>	3.950	−17.797	0.125	2

Note. - Col. (1) Filter; Col. (2) Time of NIR maximum; Col. (3) Average absolute peak magnitude; Col. (4) rms of fit in magnitudes; Col. (5) Number of SNe used in fits.

Table 8. Fit Parameters of Peak Magnitude Versus $\Delta m_{15}(B)$ for a Bimodal Distribution

Filter X	$M_X(0)$ (mag)	b_X (mag decline-rate $^{-1}$)	RMS (mag)	N_{SNe}	Subsample
(1)	(2)	(3)	(4)	(5)	(6)
Y	-18.497 ± 0.010	0.270 ± 0.160	0.181	20	2
J	-18.551 ± 0.005	0.332 ± 0.112	0.146	20	2
H	-18.418 ± 0.008	0.417 ± 0.123	0.145	20	2
Y	-18.507 ± 0.022	0.098 ± 0.261	0.137	8	5
J	-18.617 ± 0.013	0.240 ± 0.178	0.124	8	5
H	-18.451 ± 0.012	0.330 ± 0.173	0.074	8	5

Note. - Col. (1) Filter; Col. (2) Absolute magnitude for $\Delta m_{15}(B) = 1.1$ and no reddening; Col. (3) Luminosity vs. decline-rate slope; Col. (4) rms of fit in magnitudes; Col. (5) Number of SNe used in fits; Col. (6) Sample of SNe used in fit (see text).

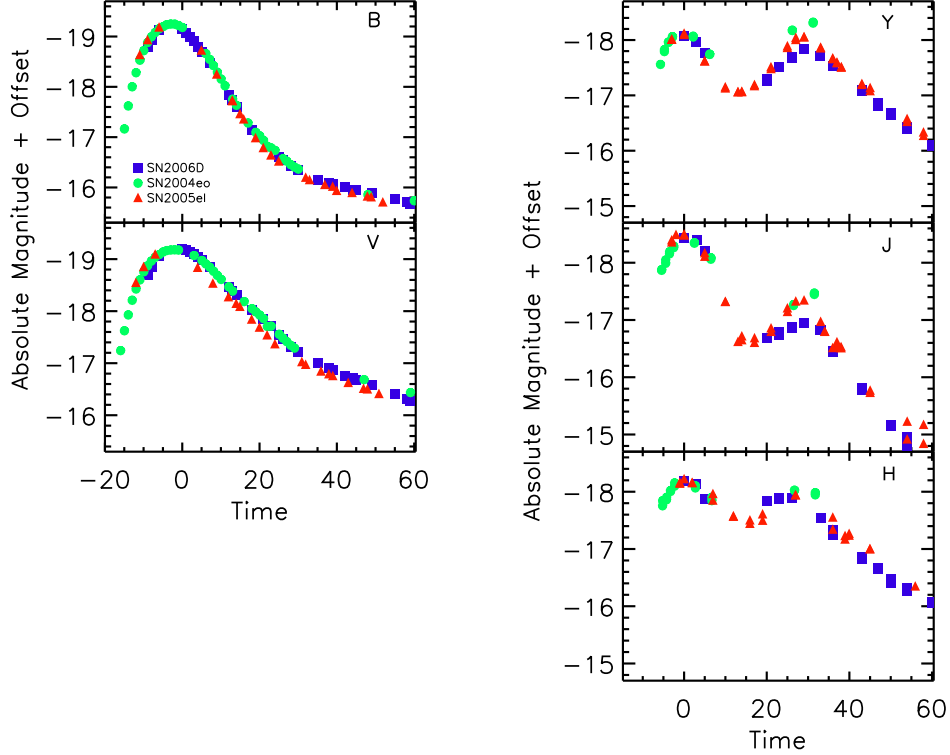


Fig. 1.— *Left*: Absolute magnitude B and V light-curves of SNe 2006D, 2004eo, and 2005el. The light-curves are shifted such that maxima agree. All SNe have similar decline-rates in the range of $\Delta m_{15}(B)=1.35 - 1.39$ mag. Blue squares represent SN 2006D, green circles represent SN 2004eo, and red triangles represent SN 2005el. Note the similarity in the B and V light-curves. *Right*: Absolute magnitude YJH light-curves of the same SNe. Again, the light-curves are shifted to a common maximum. Note the difference in the YJH light-curves, especially the difference in strength of the second maxima in the J -band.

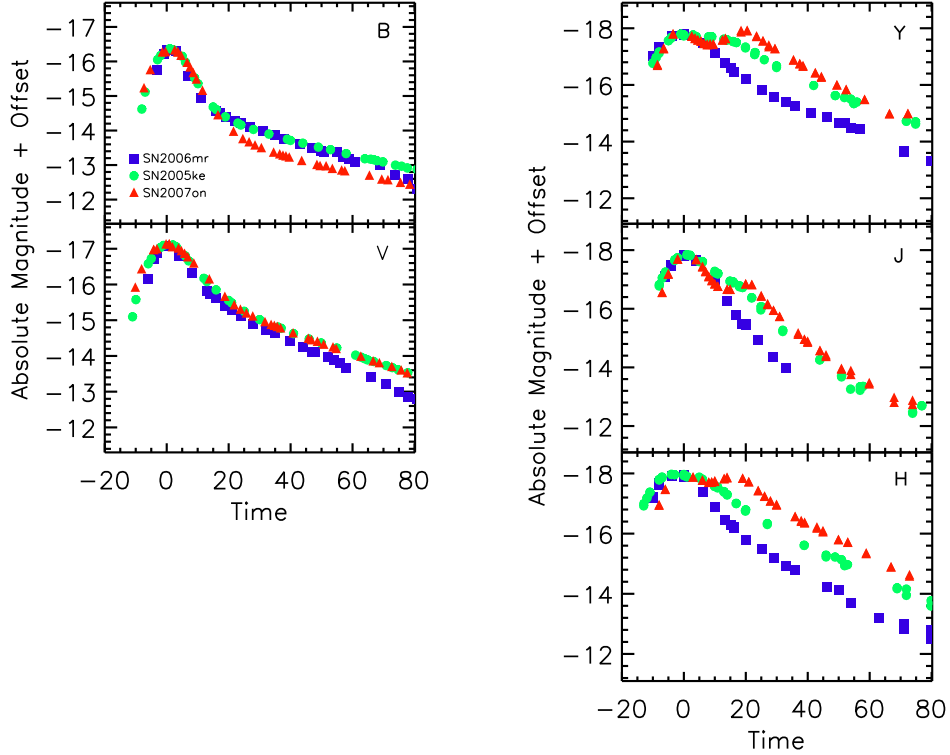


Fig. 2.— *Left*: Absolute magnitude B and V light-curves of SNe 2006mr, 2005ke, and 2007on ($\Delta m_{15}(B)=1.75-1.89$). Blue squares represent SN 2006mr, green circles represent SN 2005ke, and red triangles represent SN 2007on. The light-curves are shifted to a common maximum. As in Fig. 1, the optical light-curves are very similar. *Right*: Absolute YJH magnitude light-curves of the same SNe. The light-curves are shifted to a common magnitude. Note the large difference in the NIR light-curves, especially between SN 2007on, which shows a rise to second maxima.

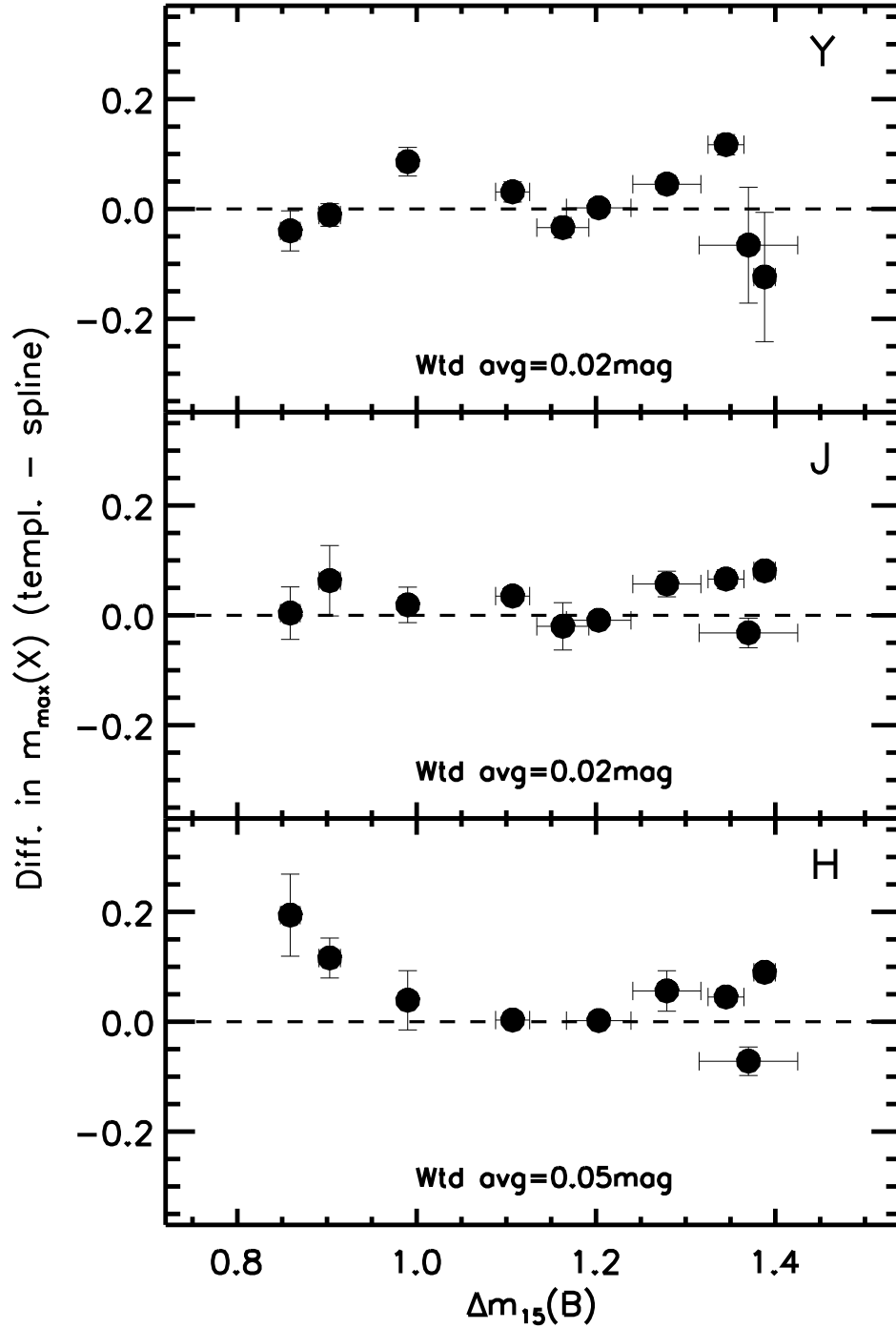


Fig. 3.— Plot of the difference in peak magnitude derived from template vs. spline fits in YJH as a function of decline-rate for objects with observed NIR maxima. Uncertainties are smaller than the points, unless shown. Evidence of systematic differences are present, but the systematic errors are not large, compared with the uncertainties in the final absolute magnitudes.

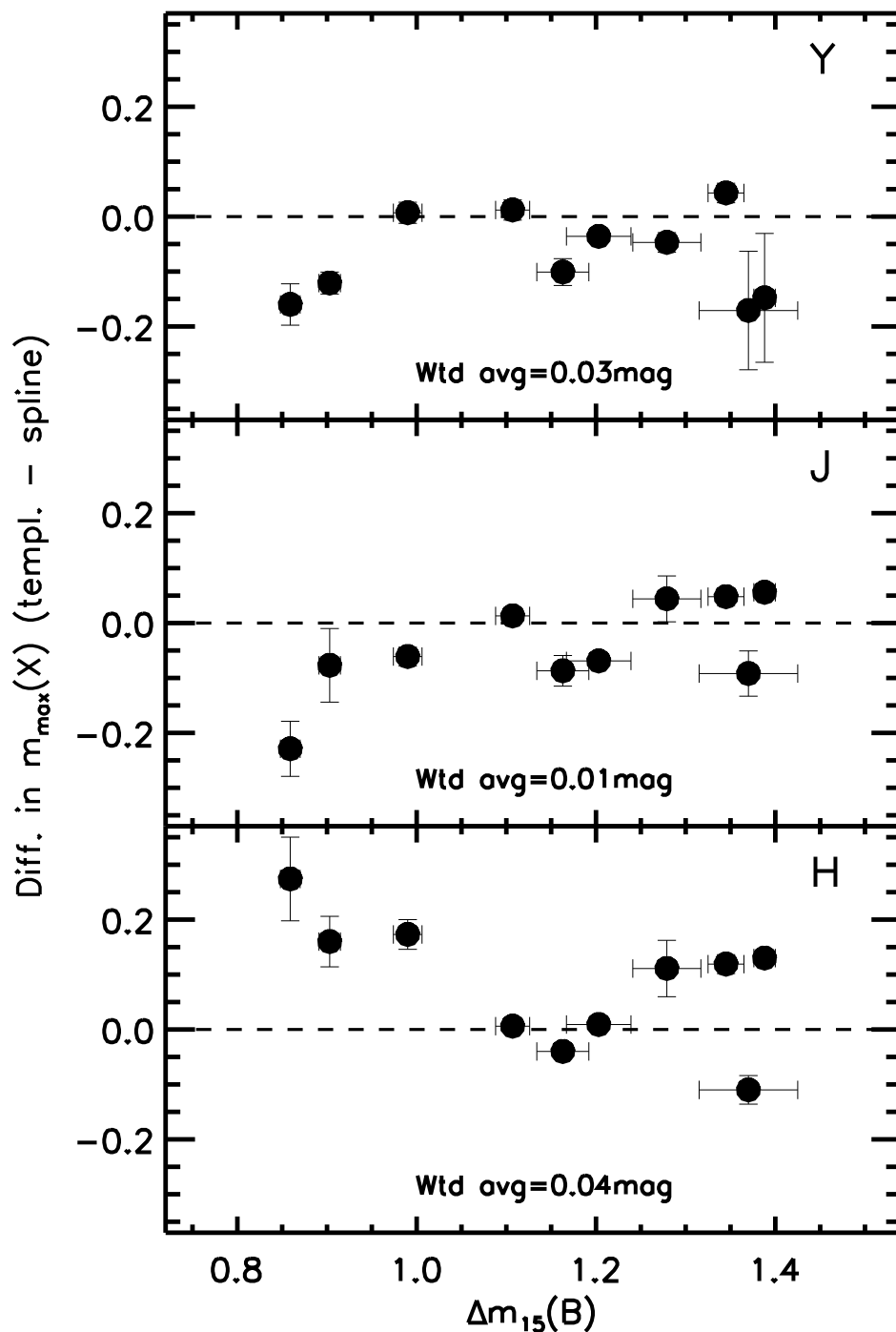


Fig. 4.— Plot of the difference in peak magnitude derived from template vs. spline fits in YJH as a function of decline-rate for SNe whose NIR observations begin within 5 days after NIR maximum. Uncertainties are smaller than the points, unless shown. The weighed averages presented here are about the same as the weighted averages found in Fig. 3, suggesting that when the observations begin within 5 days of NIR maximum, SNooPy does an adequate job of deriving peak light-curve parameters from template fits.

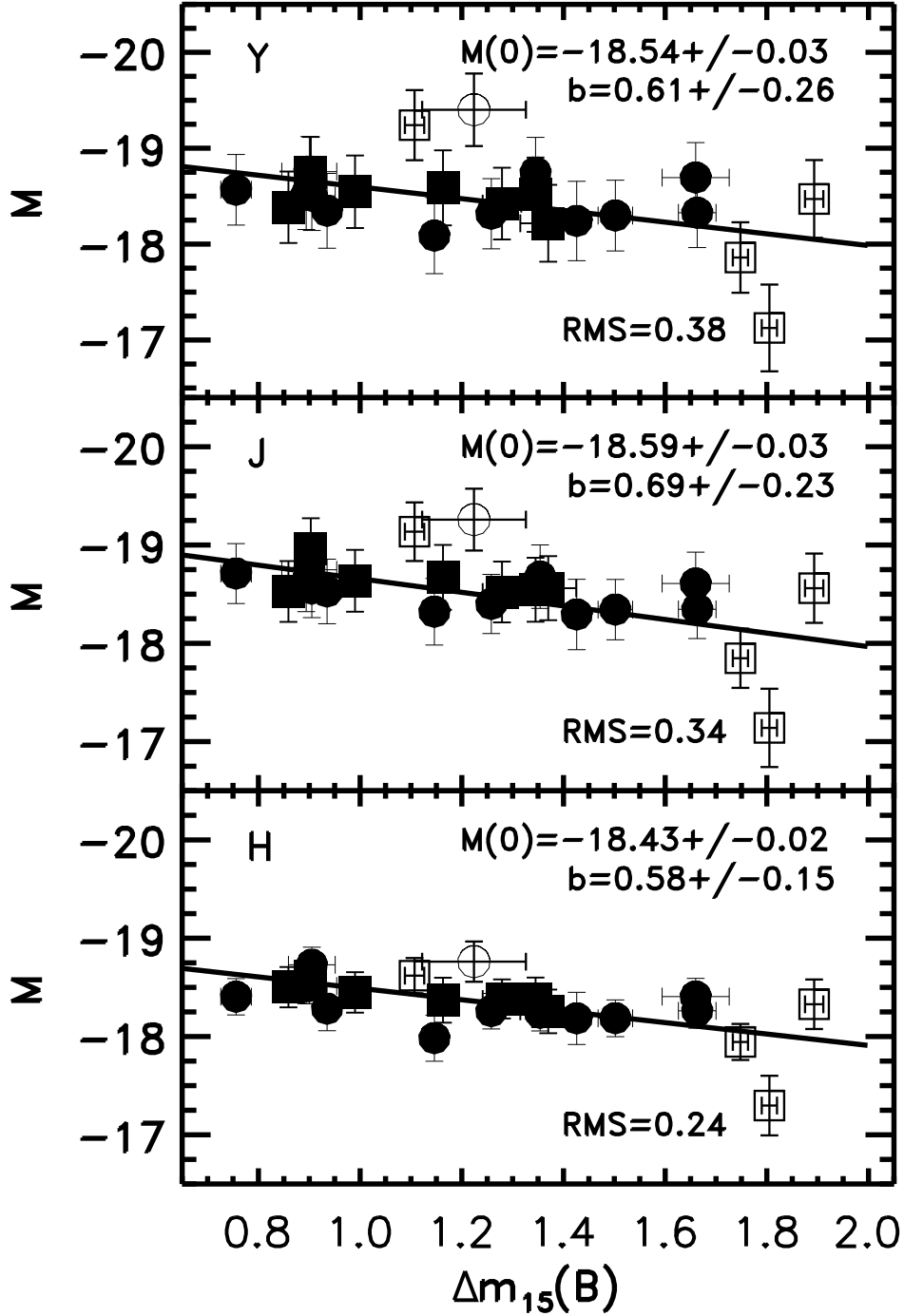


Fig. 5.— Fits of absolute YJH magnitude vs. decline-rate for subsample 1. Filled circles represent the SNe fit with a template, filled squares represent SNe fit with a spline. Open symbols represent fast-declining SNe and the highly reddened SNe. Uncertainties associated with absolute magnitude are smaller than the points, unless shown. All three of the NIR bands show a statistically significant luminosity vs. decline-rate correlation, with a dependence in all three NIR bands comparable with those found in optical bands.

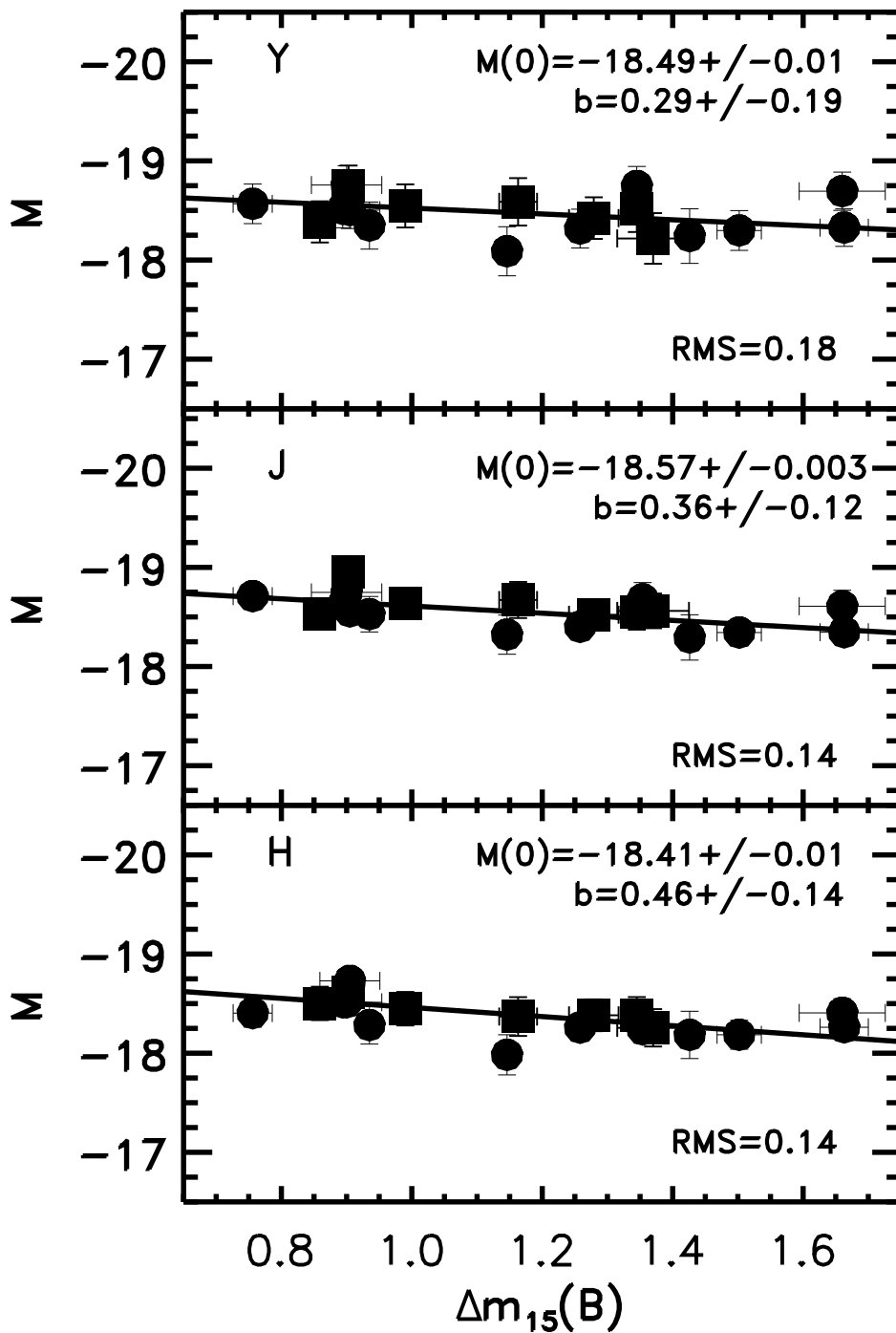


Fig. 6.— Fits of absolute YJH magnitude vs. decline-rate for subsample 2. The symbols for points are the same as those used in Fig. 5. A significantly weaker dependence of absolute peak magnitude on decline-rate is found for the YJH bands for subsample 2, and the rms dispersion decreasing significantly in all bands as well.

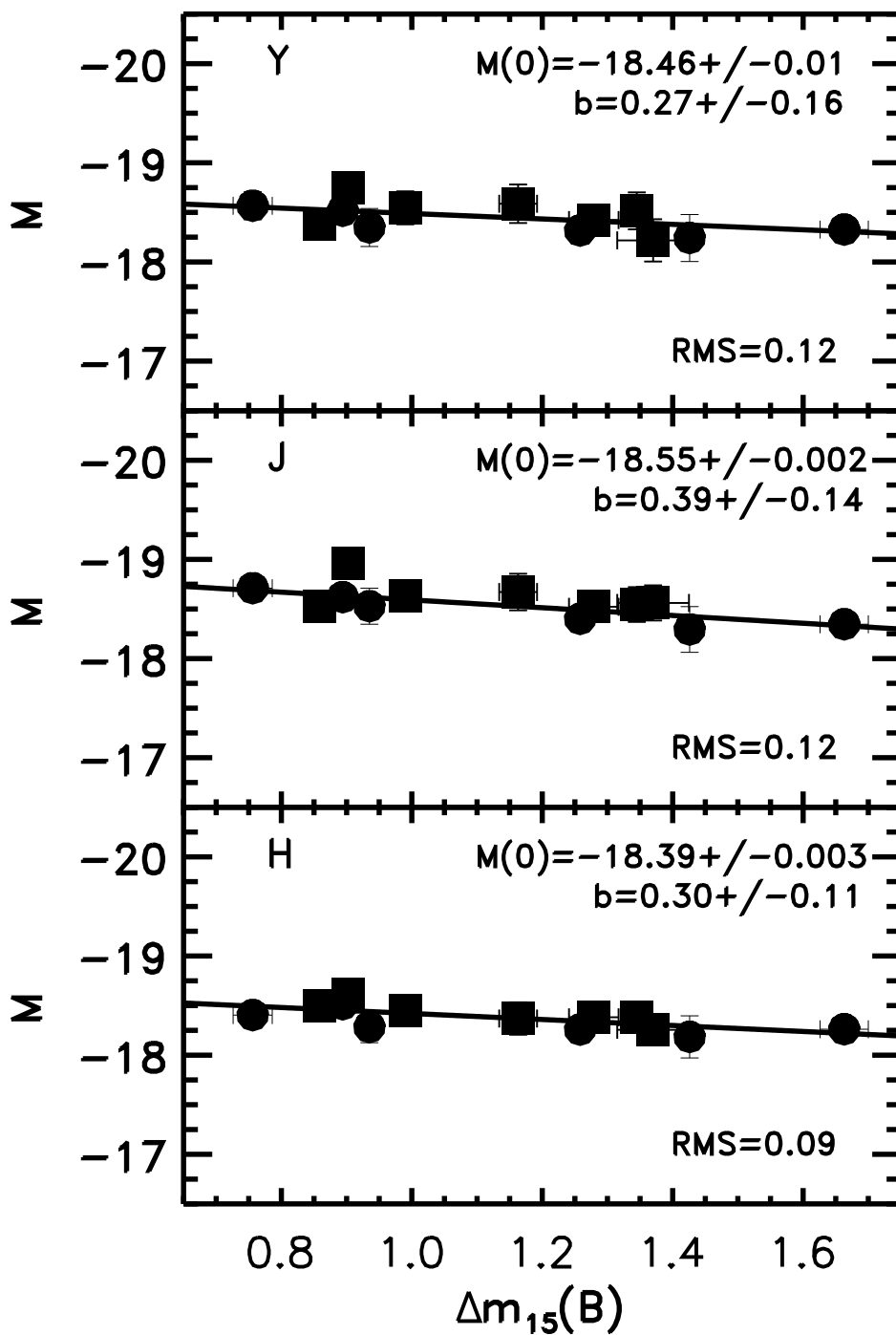


Fig. 7.— Fits of absolute YJH magnitude vs. decline-rate for subsample 3. The symbols for points are the same as those used in Fig. 5. Uncertainties associated with absolute magnitude are smaller than the points, unless shown. The Y -band shows a weak luminosity vs. decline-rate relation, while the J - and H -bands have a stronger relation, but the dependence of peak magnitude on decline-rate for subsample 3 is significantly less than in optical bands.

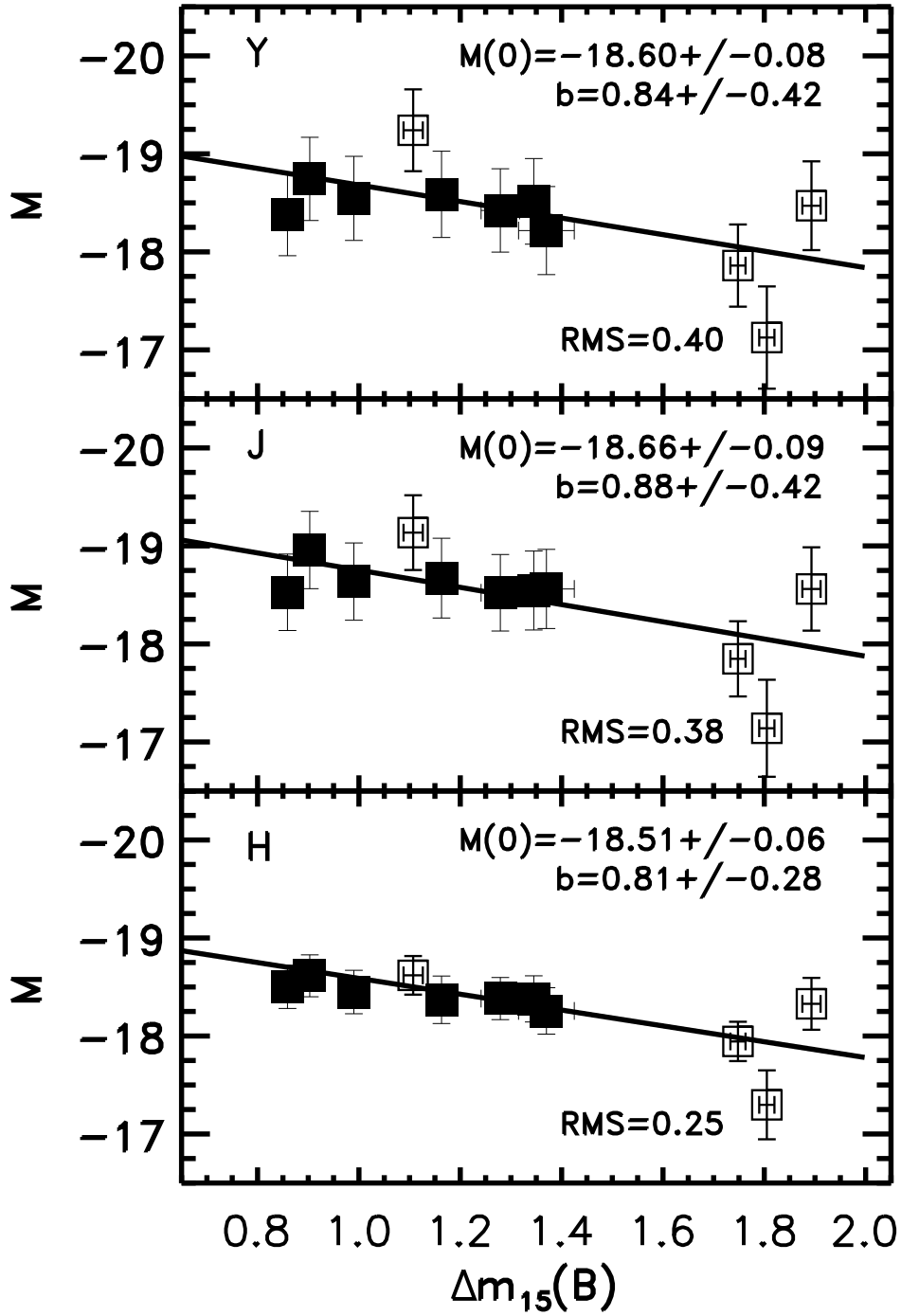


Fig. 8.— Fits of absolute YJH magnitude vs. decline-rate for subsample 4. The symbols for points are the same as those used in Fig. 5. This subsample produces the largest peak luminosity vs. decline-rate dependence of any set examined.

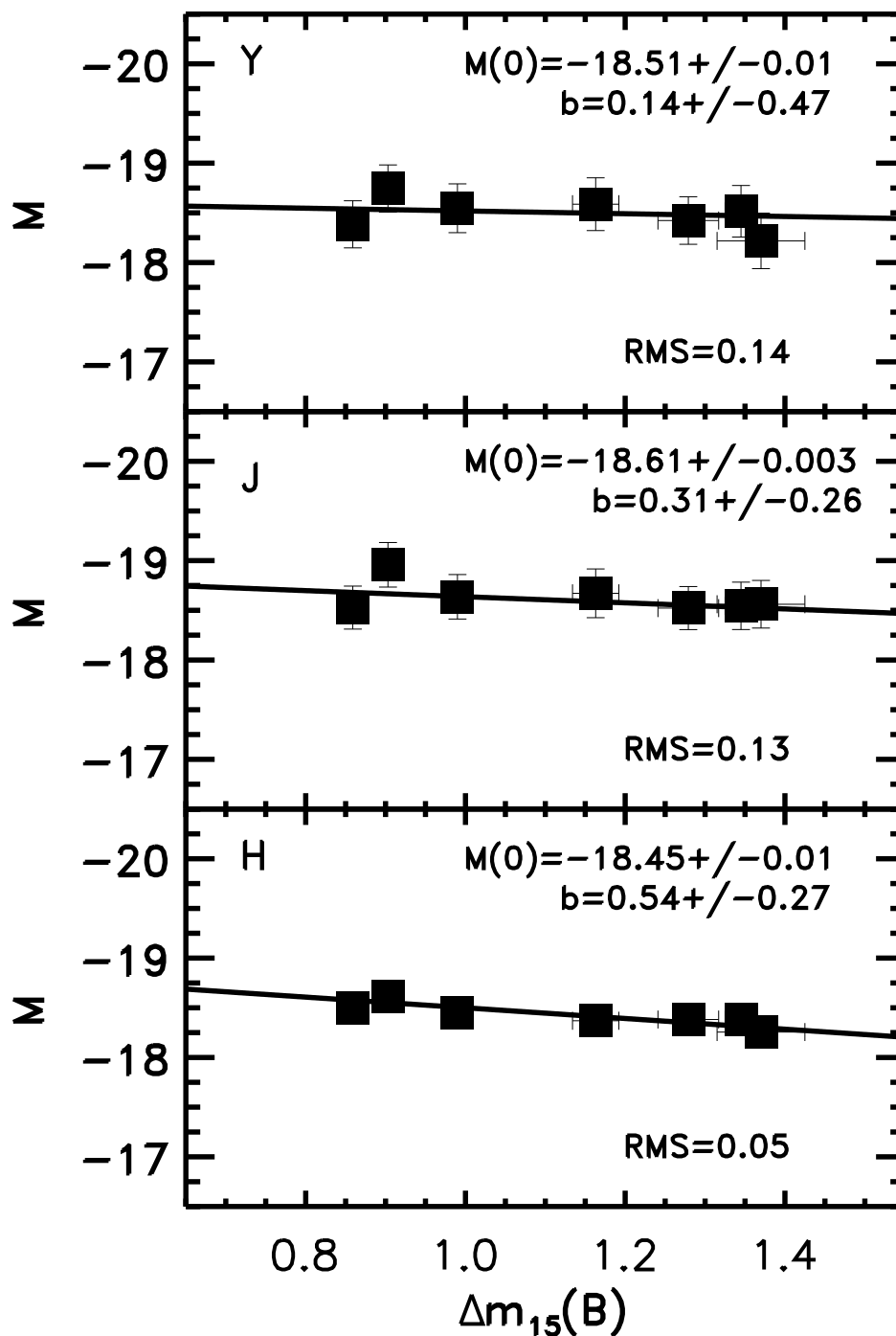


Fig. 9.— Fits of absolute YJH magnitude vs. decline-rate for subsample 5. The symbols for points are the same as those used in Fig. 5. Uncertainties associated with absolute magnitude are smaller than the points, unless shown. There appears to be little dependence of peak luminosity on decline-rate within the uncertainties for the Y - and J -bands and marginal dependence for the H -band. These results are consistent with the luminosity vs. decline-rate relations derived from subsamples 2 and 3.

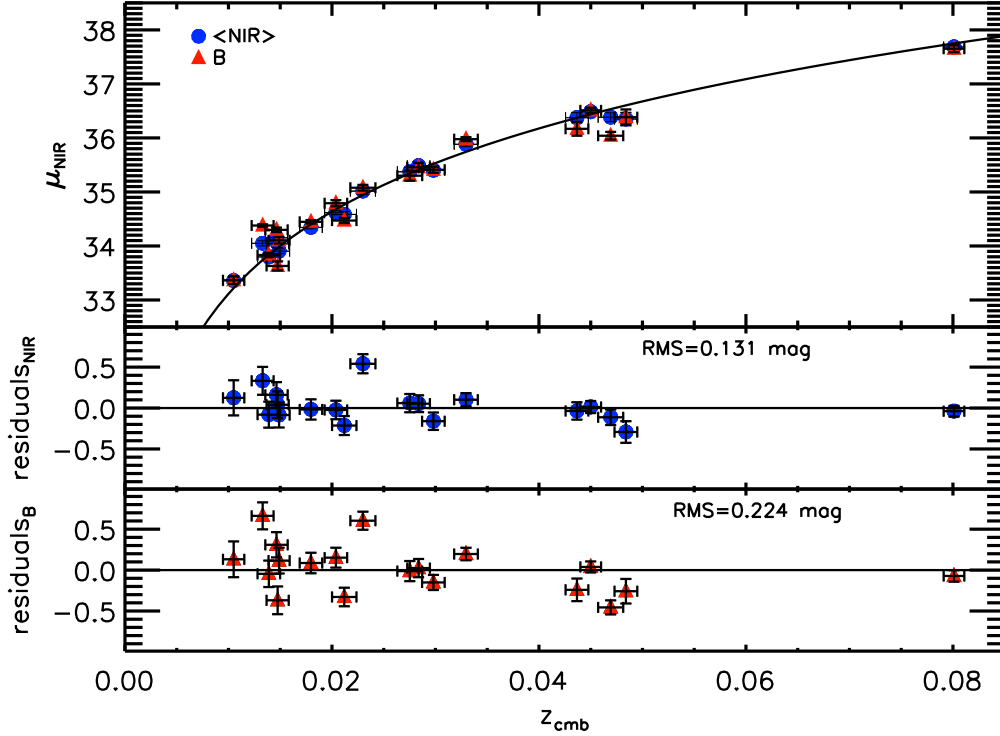


Fig. 10.— *Top*: Hubble diagram constructed from SNe and fit parameters of subsample 2. The blue circles represent the averaged NIR distance moduli for each SN, and the red triangles represent the B -band distance moduli for each SN. The solid line shows the standard cosmology redshift-distance relationship (eq. [2]). *Middle*: The NIR residuals with respect to the standard cosmology model. *Bottom*: The B -band residuals with respect to the standard cosmology model. The decrease in scatter from the optical bands to NIR bands provides strong evidence that SNe Ia in NIR bands are excellent standard candles.